Cannabinoid 1-Receptor regulation of deep and distributed subcellular processes enables neurite outgrowth

Jens Hansen[1], Arjun Singh Yadaw[1], Mustafa M. Siddiq[1], Rosa Tolentino[1], Vera Rabinovitch[1], Tong Liu[2], Hong Li[2], Joseph Goldfarb[1], Ravi Iyengar[1]*

[1]Department of Pharmacological Sciences and Systems Biology Center New York, Icahn School of Medicine at Mount Sinai, New York, NY 10029, United States.

[2] Department of Microbiology, Biochemistry and Molecular Genetics, Rutgers University, New Jersey Medical School, Newark, NY, 07103, USA.

*To whom correspondence should be addressed: Ravi Iyengar, Department of Pharmacological Sciences, 1425 Madison, Rm 12-70, Icahn School of Medicine at Mount Sinai, New York NY 10029, United States, Voice: 212-659-1707, E-mail: ravi.iyengar@mssm.edu

Abstract

Neurite outgrowth is an integrated whole cell process that represents the earliest steps in neuronal differentiation. We studied cannabinoid-1 receptor regulated neurite outgrowth to identify the different subcellular processes (SCPs) involved and how they come together to produce a whole cell response. We identified the genes that were differentially expressed after CB1 receptor stimulation. From the differentially expressed components we identified the SCPs involved and how the SCPs connect to one another both horizontally and vertically. We used these SCP networks to identify genes, which when knocked down would validate the involvement of the SCP in neurite outgrowth. We identified a varied list of SCPs including those involved in pyrimidine metabolism, lipid biosynthesis, mitochondrial transport function, mRNA splicing and stability in addition to those involved in membrane vesicle production, transport and fusion and microtubule dynamics. Overall these data and computational analyses show that the downstream SCPs required for neurite outgrowth are widely distributed and involve a range of normal cellular functions. Additionally, several of these processes can be considered distal in terms of their proximity to cell signaling pathways and the microtubule and membrane vesicle dynamics, the proximal SCPs required for neurite outgrowth. Hence we conclude that receptor regulation of neurite outgrowth is distributed and deep.

Introduction

Neuronal differentiation that results in highly connected circuits responsible for brain function starts with the formation of multiple projections called neurites. Subsequently these projections undergo further differentiation to become either axons or dendrites (Arimura and Kaibuchi 2007, Bradke, Fawcett and Spira 2012). Neurite outgrowth is considered to be among the earliest steps in neuronal differentiation. It can be triggered by wide range of extracellular signals including netrins, growth factors and ligands that regulate GPCRs (Crutcher 1986, Ziegler and Unsicker 1981, Kozlowski et al. 1989). Regulation of neurite outgrowth by GPCRs is often routed through the $G_{o/i}$ pathway. We have studied cannabinoid 1 receptor (CB1R) regulated neurite outgrowth as a model system for G protein regulated whole cell responses and have shown that signal flow from G_o through Rap to Src and STAT3 control is required (He et al. 2005). A detailed analysis of the upstream signaling network in our laboratory demonstrated the key role of transcriptional regulation and the involvement of multiple transcription factors in CB1 receptor triggered neurite outgrowth (Bromberg et al. 2008). We sought to identify the downstream mechanisms by which transcriptional control triggers neurite outgrowth. To identify the transcriptionally regulated genes involved in early neurite outgrowth we conducted RNA-Seq experiments and identified the differentially expressed genes as the starting point for mapping downstream mechanisms.

The goal of this study was to obtain a comprehensive description of the regulatory pathways involved in CB1 receptor regulated neurite outgrowth in Neuro-2A cells and rat primary cortical neurons. We had hypothesized that we might be able to track the relationships between the signaling network we had previously described (Bromberg et al. 2008) and the key cellular processes involved in neurite outgrowth: microtubule growth and vesicle transport and fusion at the growth cone (Tsaneva-Atanasova et al. 2009). However inspection of the differentially expressed genes and proteins indicated that many diverse subcellular processes (SCPs) were likely to be involved. SCPs are pathways consisting of multiple genes, with a pathway having an input node and an output effector function that might be biochemical or physiological. There are many signaling pathways, metabolic pathways and pathways with biophysical outputs in a cell. To identify SCPs and relationships between SCPs we had used standard cell biological knowledge found in textbooks such as Molecular Biology of the Cell (Alberts et al. 2015), Biochemistry (Berg, Tymoczko and Stryer 2002) and Medical Biochemistry (Rosenthal and Glew 2009) to develop a cell biological ontology called MBCO (Hansen et al. 2017). This ontology allows us to associate genes/proteins with specific SCPs and specify the relationship between SCPs required for a whole cell function such as neurite outgrowth. We analyzed the differentially expressed genes using MBCO and found a number of disparate SCPs are likely to be involved indicating that receptor regulation of neurite outgrowth was likely to be a distributed phenomenon within the cell. We also found that that many of the genes that were differentially expressed belonged to SCPs that could be considered both generally required for cell function and often viewed as part of constitutive processes. Since such SCPs are distal from the signaling networks on the proximal functions such as microtubule growth or membrane vesicle transport

we labeled them deep SCPs. We used a combination of bioinformatics analyses and dynamical modeling to understand the relationship between the SCPs in neurite outgrowth. To experimentally test the computational predictions we conducted a set of siRNA ablation studies to determine if both differentially expressed genes and computationally imputed genes that belong to SCPs that are involved in neurite outgrowth. Together these experimental and computational analyses show a complex picture where many SCPs related to many diverse functions come together to mount an integrated whole cell response: neurite outgrowth in response to CB1 receptor stimulation.

Results

Chronological activation of distributed interdependent SCPs

To characterize regulatory mechanisms that form the basis for neurite outgrowth (NOG), we stimulated the neuroblastoma cell line N2A with HU210, a potent activator of the cannabinoid 1 receptor (CB1R). CB1R stimulation increases NOG, thereby offering a model system where a well-defined receptor can trigger a whole cell response. We stimulated N2A cells for 2h, 4h, 6h and 8h with HU210 and investigated gene expression changes by bulk RNASeq (figure 1A) (Supplementary table 1).

To identify regulatory SCPs that enable NOG we subjected the differentially expressed genes (DEGs) to pathway enrichment analysis using the Molecular Biology of the Cell Ontology (MBCO) (Hansen et al. 2017). MBCO has a strict focus on cell biology and represents it in an intuitive way familiar to cell biologists, since it was designed using standard cell biology and biochemistry books as templates. SCPs are hierarchically organized and assigned to levels. SCPs of the same level describe cell biological function of similar details. Higher level SCPs (i.e. SCPs with lower level numbers) describe more general sub-cellular functions, lower level SCPs (with higher level numbers) more detailed sub-cellular functions. To construct networks of SCPs, the hierarchical tree is enriched using a unique MBCO algorithm that predicts weighted horizontal interactions between SCPs of the same level that lie within and beyond the annotated hierarchy. These interactions enable the dynamic characterization of functionally dependent SCP-networks from experimentally obtained gene lists that underlie the integrated whole cell response. This enrichment algorithm is called dynamic enrichment analysis and serves as a valuable addition to standard enrichment analysis using Fisher's Exact Test. Briefly, dynamic enrichment analysis searches for all level-2 or level-3 SCPs that contain at least one input gene and combines them to SCP-unions, if they are horizontally connected with a minimum connection weight. The unions are added as function-specific SCPs to the original set of SCPs and the new function-specific MBCO is used for enrichment analysis of the gene list. Results are ranked by p-value and the top 3 level-2 or top 5 level-3 predictions (that are either single SCPs or SCP-unions) are connected with each other based on all MBCO horizontal interactions to generate SCP-networks.

We analyzed up- and down-regulated genes at each time point after CB1 receptor activation of Neuro-2A cells using MBCO and standard and dynamic enrichment analysis (Figure 1B-C, Supplementary figure 1). Since we were interested in obtaining near comprehensive maps of downstream mechanisms we looked for all identifiable cellular mechanisms that can drive cellular state change and used two different minimum fold change cutoffs for the DEGs submitted to enrichment analysis. We used a more stringent cutoff for DEGs that we submitted to dynamic enrichment analysis to identify SCP networks underlying whole cell state changes, and a more relaxed cutoff for DEGs submitted to standard enrichment analysis (minimum $\log_2$(fold change) = +/- $\log_2(1.5)$ for dynamic and +/- $\log_2(1.3)$ for standard enrichment analysis (Figure 1A)).

Enrichment results predicted multiple SCPs and SCP networks that *suggest* the activation of different sub-cellular functions in a chronological order that matches their dependencies (Figure 1B) (suppl. table 2 and 3). SCP-networks at 2h describe microtubule and centrosomal re-arrangements that could be associated with preparations of the centrosome that localizes at the hillock of the future axon at an early stage of NOG (de Anda et al. 2010, Higginbotham and Gleeson 2007, Tang and Marshall 2012) (suppl. figure 1A/B). Genes associated with nuclear chromatin condensation are down-regulated, suggesting that at this stage the cell prepares for increased gene expression by increasing chromatin accessibility for transcription. Concordantly, up- and down-regulated SCP-networks at 4 hours suggest an increase of gene expression, mainly via up-regulation of ribosomal proteins and down-regulation of CCR4-NOT complex subunits that are involved in bulk mRNA degradation and polymerase II suppression (suppl. figure 1C). Lamellipodia formation is up-regulated (suppl. figure 1D), in agreement with morphological observations that neurites emerge from lamellipodia that form at the earliest stages of NOG (Govek, Newey and Van Aelst 2005). Activity changes in mitochondrial processes indicate mitochondria also prepare for outgrowth (suppl. figure 1D), in agreement with the observation that mitochondria accumulate at the hillock of the future axon before its major growth phase (Bradke and Dotti 1997, Mattson and Partin 1999). Up-regulated pyrimidine synthesis and salvage can support gene expression, since it generates the building blocks for mRNA synthesis and suggests that the cell is preparing for an increase in lipid membrane production, since the pyrimidine nucleoside triphosphates CTP and UTP are cofactors during membrane lipid synthesis (Garavito, Narváez-Ortiz and Zimmermann 2015). The up-regulated SCP-network at 6 hours describes microtubule-based vesicle trafficking between the Golgi apparatus and the plasma membrane (figure 1C, suppl. figure 1E), suggesting a cellular focus on membrane delivery from the lipid synthesis site in the cell body to the growth cone where new membrane is added to the growing neurite shaft (Pfenninger 2009, Nakazawa et al. 2012). In agreement, standard enrichment analysis (suppl. figure 1F) predicted up-regulation of membrane lipid metabolism. Up-regulated microtubule plus end tracking further supports that DEGs at 6h refer to the main neurite growth phase that is characterized by parallel and interdependent growth of the neurite shaft and microtubule neurite scaffold. 8h DEGs enrich for multiple SCPs and SCP-networks, including the up-regulation of splicing activities and further modification of vesicle

trafficking (including retrograde vesicle trafficking) and membrane lipid synthesis (suppl. figures 1G/H).

DNA repair processes are predicted to be down-regulated after 2h, 4h, and 6h HU210 treatment (Suppl. figures 1A/C/E). Such SCP activities could be involved in the regulation of gene expression (Madabhushi et al. 2015).

Neurite outgrowth requires many metabolic processes

To document the involvement of the predicted SCPs in neurite outgrowth we selected representative genes for siRNA knock down (figure 2). Our aim was not to analyze if a certain gene is involved in a particular SCP, but if a particular SCP is involved in NOG. Therefore, when possible, we selected genes whose knock down has been shown to influence the corresponding SCP in other cell types, independent of its transcriptional regulation during NOG. Indeed, most of the genes selected for siRNA knockdown were not identified as DEGs in our RNASeq screening approach (Table 1).

Primary rat cortical neurons were seeded on microfluidic chambers that contain two sides that are separated by a microgroove sidewall (figure 2A). Plated on one site of the chamber, the cell bodies cannot cross to the other side, but their neurites can grow through small slits in the sidewall into the other side, allowing an easy quantification of outgrowth length. After siRNA transfection we waited for 48h to allow degradation of the targeted protein and performed axotonomy to reset neurite growth length in all chambers to 0 (i.e. to the microfludic sidewall). Neurite outgrowth was documented and quantified after another 48h. Average growth intensity at 750 µm from the microgroove was quantified and compared between control and knock down neurons. Typically the effects of the knockdown were small; hence we used multiple independent biological replicates to validate the effects.

We could document the involvement of multiple SCPs that we identified in our RNASeq screening approach (Figure 2B). Among these were SCPs that can be directly linked to neurite shaft growth such as membrane lipid production and membrane delivery to growth cone via vesicle trafficking, as well as SCPs that describe deep regulatory functions that contribute to neurite outgrowth on a lower more basal level (e.g. mRNA splicing).

Pyrimidine Biosynthesis Pathways

Pyrimidine synthesis and salvage was predicted to be up-regulated after 4h HU210 treatment. Pyrimidines are substrates for multiple sub-cellular pathways such as DNA and RNA synthesis and are co-factors during the synthesis of phosphatidylethanolamine (PE), phosphatidylcholine (PC) and complex gangliosides (Figure 3A) (Garavito et al. 2015). The up-regulation of

pyrimdine synthesis and salvage could therefore support increased gene expression by delivering the building block for mRNA synthesis. Additionally, an increased pool of the pyrimidine nucleoside triphosphates CTP and UTP could support phospholipid and ganglioside synthesis, SCPs that are up-regulated after 6h HU210 treatment. CTP is a co-factor for neuronal phosphatidylethanolamine- and -glycin synthesis via the Kennedy pathway (Vincenzetti et al. 2016) and uridine induces intracellular CTP increase and neurite outgrowth (Pooler et al. 2005). UTP and CTP are co-factors for ganlioside synthesis (Sandhoff and Sandhoff 2018). Though the pyrimidine de novo synthesis was also up-regulated, we could only document the dependence of NOG on pyrimidine salvage (Tymp), but not on pyrimidine de-novo synthesis (Cad, Dhodh). These results are in agreement with the observation that pyrimidine de novo synthesis is expensive, so pyrimidine recycling should be favored to maintain a sufficient pool for pyrimidine dependent pathways (Vincenzetti et al. 2016). The source for recycled substrates might either be pyrimidine metabolites that were generated in the same cell (e.g. after DNA/RNA degradation) or metabolites that were produced by astrocytes, since we used astrocyte conditioned media, to generate an environment that resembles the in-vivo situation in the CNS.

Lipid Biosynthesis Pathways

The distribution of up- and down-regulated genes within membrane lipid synthesis pathways suggests an increase in the synthesis of ceramide and complex gangliosides (Figure 3B) and a shift in phospholipid synthesis from phosphatidylcholine (PC) to phosphatidylethanolamine (PE) and phosphatidylserine (PS). Genes involved in lipid synthesis pathways are up-regulated in parallel to genes involved in vesicle transport, suggesting the functional coupling of both pathways for membrane synthesis and delivery to the growth cone.

Complex gangliosides contribute to about 10 to 20% of lipids in neuronal membranes (Posse de Chaves and Sipione 2010) and are synthesized using ceramide as a substrate (Yu et al. 2004). They are primarly localized at the outer leaflet of the plasma membrane (Yu et al. 2011), suggesting that ceramide and ganglioside synthesis are up-regulated to generate the building blocks of the outer leaflet of the growing neurite. In agreement with these observations, we find that knock down of genes that are involved in ganglioside synthesis, either as an enzyme (Ugcg) (Daniotti and Iglesias-Bartolomé 2011) or as a lipid transport protein (Plekha8) that directs glycosylceramide from the cis-Golgi to the synthesis site of complex gangliosides at the trans-Golgi (D'Angelo et al. 2007, Yamaji et al. 2008, Lannert et al. 1998), inhibit or show a tendency to inhibit neurite outgrowth. In contrast, the knock of Col4a3bp, a lipid transport protein that directs glycosylceramide to sphingomyelin synthesis sites at the Golgi (Hanada et al. 2003, Hanada et al. 2009, Yamaji et al. 2008) shows conflicting effects on NOG, that could be the result of neuronal sphingomyelin synthesis at a non-Golgi location (Sadeghlar, Sandhoff and van Echten-Deckert 2000, van Echten et al. 1990).

PE and PS mainly localize to the inner leaflet of the plasma membrane (Fadeel and Xue 2009), suggesting that the up-regulation of enzymes involved in PE and PS synthesis via the Kennedy pathway increases the production of the building blocks of the inner leaflet of the growing neurite. PC, the most abundant phospholipid in cell membranes, is largely localized at the ER (Tracey et al. 2018) and serves as a storage reservoir for choline that is used for neurotransmission (Blusztajn et al. 1987a, Blusztajn, Liscovitch and Richardson 1987b). The two different arms of the Kennedy pathway that synthesize PE (that can be converted into PS) and PC both utilize Diacylglycerol (DAG) as a substrate and the pyrimidine nucleoside triphosphate CTP as a co-factor (Vincenzetti et al. 2016). The predicted down-regulation of PC synthesis might further favor the production of PE and PS by increasing the availability of both molecules for PE synthesis. Knock down of Pcyt2, an enzyme involved in PE synthesis via the Kennedy pathway, decreases NOG. Similarly, the knock down of Pcyt1a, an enzyme involved in PC synthesis via the Kennedy pathway, also decreases or shows a tendency to decrease NOG. Though our DEGs suggest a shift from PC to PE and PS synthesis to increase neurite membrane production, NOG still depends on a sufficient supply of PC as the most abundant phospholipid in cell membranes (Carter et al. 2008).

Mitochondrial Functions

Differential expression of genes at 4h HU210 that are involved in structural mitochondrial organization suggest a shift from Rhot1 to Rhot2 mediated anterograde mitochondrial transport, a shift from mitochondrial fission to mitochondrial fusion, the down-regulation of mitochondrial gene expression and activity changes in SCPs that are involved in mitochondrial protein import, mitochondrial gene expression and oxidative phosphorylation (Figure 3C). Knock down of 4 mitochondrial genes inhibited or showed the tendency to inhibit neurite outgrowth, documenting the importance of the SCPs mitochondrial anterograde transport, fusion, translation and protein import. Mitochondria populate the growing neurite where they increase their length through fusion (Voccoli and Colombaioni 2009). Our results suggest that mitochondria are first prepared for populating the neurite before the neurite enters its major growth phase, since mitochondrial genes are up-regulated before the up-regulation of genes involved in membrane synthesis and vesicle trafficking. This interpretation complements morphological observations showing mitochondria, peroxisomes and Golgi vesicles accumulation at the base of that neurite that becomes the future axon before it enters its major growth phase (Mattson and Partin 1999, Bradke and Dotti 1997).

Regulation of mRNAs

In parallel to the up-regulation of ribosomal genes after 4h HU210 treatment, we observed multiple downregulated genes that participate in bulk mRNA degradation (figure 3D). Our results suggest that an increase in gene expression that is needed for continuous synthesis of neurite components for the following neurite growth phase (6h) is facilitated by an increase in ribosomal translation and mRNA lifetime. Down-regulated genes after 4h HU210 treatment are part of multiple SCPs that participate in mRNA degradation at multiple consecutive steps (Norbury 2013): initial mRNA-polyA tail trimming, bulk mRNA polydeadenylation by the CCR4-NOT complex, mRNA decapping and exosome-independent degradation of deadenylated and polyuridylated mRNA (De Almeida et al. 2018). The CCR4-NOT complex regulates numerous steps during mRNA biogenesis including transcription, mRNA export and mRNA degradation (Collart 2016, Doidge et al. 2012, Ukleja et al. 2016, Villanyi and Collart 2015). Three of the five down-regulated CCR4-NOT complex subunits have 3'-5' poly(A) exoribonuclease activitity (Doidge et al. 2012), suggesting that down-regulation of these complex components increases mRNA lifetime.
siRNA knock down of the putative catalytic component Dis3 of the exosome complex (Kilchert, Wittmann and Vasiljeva 2016, Siwaszek, Ukleja and Dziembowski 2014) that is involved in another degradation pathway of polydeadenylated mRNA slightly decreases NOG, indicating that mRNA degradation, possibly of mRNAs that contain errors, is still a necessary function to secure neurite outgrowth.

Components of the splicing machinery are down-regulated after 4h HU210 treatment, i.e. at the timepoint where other enrichment results suggest an increase in gene expression, and are up-regulated after 8h HU210 treatment, i.e. after the up-regulation of the machinery for neurite shaft and scaffold growth at 6h. This chronological order suggests that down-regulation of the splicing machinery after 4h HU210 treatment contributes to the increase of gene expression to ensure continuous production of proteins at the cell body for the following intial neurite growth phase. The late timepoint of the up-regulation of the splicing machinery at 8h suggest that a higher concentration of splicing machinery components is needed to contribute to advanced neurite growth phase. Axonal growth cones contain a reservoir of translationally silent mRNAs (Kim and Jung 2015) and the machinery for local translation, protein folding and posttranslational modification (Estrada-Bernal et al. 2012). More than half of the neurite-localized proteome might have been generated by local mRNA translation (Zappulo et al. 2017). Alternative splicing of 3' UTRs localizes neuronal mRNA molecules to neurites (Taliaferro et al. 2016). Restriction of spliceosomal components alters splicing of a subset of mammalian mRNAs with week 5' splice sites (Wickramasinghe et al. 2015). Our results might suggest that low concentrations of the splicing machinery favor splicing to produce mRNA for protein production in the cell body, while high concentrations increase alternative splicing to generate mRNAs that are transported into the neurite for local protein production.

The involvement of splicing in neurite outgrowth was documented by our knock down results. Knock down of the spliceosomal components Sf3a2 and Snrnp70 inhibits NOG.

Membrane Vesicle Transport

DEGs related to vesicle transport processes are related to multiple steps that describe vesicle transport processes between the plasma membrane, endosome and TGN (Figure 3E). Our siRNA screening supported this observation, since we could document that multiple SCPs ranging from vesicle loading on the microtubule after budding at the TGN (Burgo et al. 2012), vesicle exocytosis and retromer based endosomal sorting (Gallon and Cullen 2015, Zhang et al. 2018). The gene Vps35 is a main component of the retromer that is involved in protein sorting from the endosome to the plasma membrane and to the Golgi. Its knock down shows a tendency to decrease NOG at 750 μm distance from the microgroove sidewall, while neurite density at 500 μm is clearly lower after Vps35 knock down (data not shown). Knock down of SNX2 shows a tendency to increase NOG. For retromer function this gene shows redundancy with SNX1 (Rojas et al. 2007), so its knock down might not influence retromer function at all. In combination with the observed up-regulation of genes involved in retrograde transport from the endosome to the Golgi, these results indicate that an increase in back transport from the growth cone to the TGN is needed to increase NOG outgrowth velocity.

To further investigate this counter-intuitive finding we used our multicompartment ODE model that integrates membrane production, membrane delivery to the growth cone via vesicle transport and microtubule growth during NOG (Yadaw et al. 2017) to understand how membrane back transport regulates NOG. In this model we start with the postulate that individual SCPs need to be in balance to achieve neurite outgrowth without violation of predefined model constraints. The model simulates anterograde (forward) and retrograde (backward) vesicle trafficking between the TGN and the growth cone (Figure 4A). Anterograde vesicles bud at the TGN and move through the neurite shaft to the growth cone cytoplasm via kinesin mediated transport along the microtubules. Kinesin is attached to the vesicles via kinesin receptors that are integral parts of the vesicle membrane. Anterograde vesicles within the growth cone cytoplasm fuse with the growth cone plasma membrane after SNARE complex formation between vesicle(v)-SNAREs V and target(t)-SNAREs at the plasma membrane. Any additional membrane at the growth cone is added to the neurite shaft, causing its growth. Retrograde vesicles are generated via endocytosis at the growth cone membrane, transported backwards along the microtubules via dynein mediated vesicle transport into the cell body cytoplasm and fuse with the TGN.

Part of our NOG model is an analytical solution that predicts kinetic parameter sets that allow NOG growth under a certain velocity without violation of SCP model constraints.

Using our dynamic model, we could predict that the total number of vesicle(v)-SNAREs and vesicle kinesin receptors in the neuronal cell increases with increasing NOG velocity (Figure

4B/C). The higher the outgrowth velocity the more vesicles need to be transported to the growth cone. Consequently, higher velocities demand more v-SNAREs and kinesin receptors to equip the anterograde moving vesicles. Our model predicts that the amount of needed v-SNAREs and kinesin receptors rapidly increases, if the backtransport rate lies below a certain threshold. Below a second lower threshold it is not possible anymore to achieve NOG without violation of the model constraints (empty spots on the right sites of the walls in figure 4A and 4B). Any v-SNAREs and kinesin receptors that are brought to the growth membrane need to be back transported to the TGN to be available for the next set of anterograde moving vesicles. The binding spots for v-SNAREs and kinesin receptors on a vesicle are limited. Consequently, to secure the back transport of a sufficient amount of v-SNAREs and kinesin receptors at higher outgrowth velocities more vesicles have to move backwards, increasing the total membrane back transport rate.

Discussion

Several previous studies in mice (Sekine et al. 2018, Tedeschi et al. 2016) and in worm (Chisholm et al. 2016) have shown differentially expressed genes during axonal regeneration after injury encode components of numerous cell signaling pathways including those involved in synaptic plasticity as well as SCPs involved in vesicle transport. A genome wide screen during regeneration identified a distinct set of genes including members of the SOCS family, inhibitors of signaling through Stat3. This finding is in agreement with our previous finding of an essential role for Stat3 in neurite outgrowth (Bromberg et al. 2008). Another prominent gene identified in the genome wide screen was Rab27 a protein involved vesicle transport (Sekine et al. 2018). We started with a different approach where our goal was to identify genes regulated by a GPCR, the CB1 receptor, so that we could identify the SCPs involved and how they connected with one another to produce a whole cell function. So it was not entirely unexpected that these differentially expressed genes are somewhat different. In looking through the SCPs and the differentially expressed genes that are involved in it it became clear that CB1 receptor regulation of neurite outgrowth is both deep and distributed (Figure 5). By distributed we mean that a wide range of SCPs are involved. By deep we mean SCPs involved are often part of general cellular function and not necessarily selective for neurite outgrowth or even neuronal functions. This includes regulation of pyrimidine metabolism, mitochondrial transport and regulation of RNA stability. Regulation of these SCPs can affect many cellular responses in many different cell types and hence it is possible that such deep regulation may be a common feature of cell state change. Future experiments in other cell types will be needed to determine if these same SCPs are involved on other cell state change events.

In order to validate the functional role of the SCPs inferred from differentially expressed genes we used an orthogonal strategy that had three parts. First, we conducted the siRNA based knockdown studies using rat cortical neurons in primary culture. Second, we studied neurite

outgrowth in microfluidic chambers where we could sever initially growing neurites and then measure neurite growth in a standardized way. Although it was not our intent to study the SCPs involved in axonal regeneration after injury, our experimental approach allows to reasonably suggest that the SCPs we identify could play a role in axonal regeneration. Third, we did not only knock down genes that were differentially expressed but also genes, whose expression levels did not change but were within SCPs that we computationally inferred to be relevant for neurite outgrowth. This approach allowed us to focus on SCPs rather than on individual genes. Overall the siRNA based knockdown experiments allowed us to identify a diverse set of SCPs required for neurite outgrowth. It should be noted that the magnitude of the effects are modest, both for the differentially expressed genes as well as effect of knockdown. This is not surprising given the wide range of SCPs involved.

For many of the deep SCPs we were able to find previous studies that had individually implicated a role for the SCPs in neurite outgrowth. These include phospholipid biosynthesis (Carter et al. 2008) and mitochondrial functions (Cheng, Hou and Mattson 2010). Nevertheless, our findings cannot be interpreted as definitive proof that the SCPs we describe here are involved in neurite outgrowth in all conditions and in all species. Such proof will have come from future in depth experiments that analyzes the role of the SCP of interest in terms of the different genes involved. Thus to some extent our interpretation can be considered to be experiment based hypothesis generators. Even with this cautious interpretation we have in this study described how a receptor can trigger a whole cell response by regulating a diverse set of SCPs and the relationship between the SCPs in enabling the whole cell response - neurite outgrowth.

Methods:

Cell culture

mRNA was prepared from 2 to 3 pooled experiments to achieve a sufficiently high amount of mRNA. Briefly, for each experiment 1 million Neuro2A cells were seeded on each of eight 15cm dishes and cultured for about 24h in MEM (supplemented with 10% FBS, sodium pyruvate and 1% Penicillin/Streptomycin). Low cell counts ensured low confluence that leaves sufficient space for neurite outgrowth. After 16h starvation in serum free MEM supplemented with 0.1% Bovine Serum Albumin (BSA) we added HU210 (dissolved in sodium pyruvate DMSO) to the media in a final concentration of 2 μM. Control cells were treated with equal volumes of drug free DMSO. Cells were incubated for 2, 4, 6 and 8h before replacement of the media by 8ml TRIZOL to stop the experiment. Trizol dissolved cells were collected and frozen at -80C.

RNASeq - sample preparation and sequencing

RNA was prepared using the standard TRIZOL protocol. RNA was subjected to quality control via Agilent Bioanalyzer. All samples had an RNA integrity score of 10. 40 μg of total RNA was used for each sample. mRNA was purified from the RNA using Dynabeads mRNA Purification Kit and fragmented via sonication using the Covaris E210. cDNA libraries were prepared as described previously (Nagalakshmi et al. 2010, Quail et al. 2008, Quail et al. 2009). Fragments of 200 to 300 base pairs length were selected via gel size selection. cDNA libraries were subjected to sequencing using an Illumina HiSeq 2000 machine. Each sample was subjected to a single lane, yielding ~100 million reads per sample.

Identification of differentially expressed genes (DEGs)

Raw reads were aligned to the mouse reference genome mm9 using Tophat 2.0.8., samtools-0.1.7 and bowtie 2.1.0. Tophat was used with the ensemble GTF file as a gene annotation reference and the option 'no-novel-juncs'. Output BAM files were directly subjected to differential gene expression analysis using Cufflinks with the options 'multi-read-correct', 'upper-quartile norm' and 'frag-bias-correct' against the mm9 genome. DEGs were identified based on adjusted p-value (FDR 5%) and a minimum fold change ($\log_2[(FPKM_{HU210}+1) / (FPKM_{DMSO} + 1)] >= \pm \log_2(1.5)$ or $\pm \log_2(1.3)$).

Standard and dynamic enrichment analysis

Up- and down-regulated genes were subjected to pathway enrichment analysis using Fisher's Exact Test and the Molecular Biology of the Cell Ontology (Hansen et al. 2017) (https://github.com/SBCNY/Molecular-Biology-of-the-Cell). Since mitochondria SCPs are distributed over various MBCO branches (i.e. they are children of multiple level-1 SCPs such as 'Organelle organization', 'Energy generation and metabolism of cellular monomers' and 'Transmembrane protein import and translocation') we generated a new level-1 mitochondria

SCP (Mitochondria structural organization) and defined it to be the parent of all mitochondria related level-1 and level-2 SCPs. It was populated with all genes of its children SCPs.

Significantly up- or down-regulated genes with a minimum $\log_2$ fold change of $\pm \log_2(1.5)$ were separately subjected to dynamic enrichment analysis, using MBCO level-2 and level-3 sub-cellular processes (SCPs). MBCO contains predicted horizontal interactions between SCPs of the same level that can be ranked by their interaction strengths and complement the hierarchical vertical relationships between parent and child SCPs. Dynamic enrichment analysis uses these horizontal interactions to predict SCP networks that underlie whole cell function. Briefly, dynamic enrichment analysis identified those level-2 or level-3 SCPs that contain at least one input gene (e.g. an up-regulated gene) and combines 2 or 3 of the identified SCPs to SCP unions, if they are strongly connected. To generate level-2 SCP-networks we use the top 20% horizontal SCP interactions, to generate level-3 SCP networks the top 25% interactions. Generated SCP unions are added as new context specific SCPs to the ontology and the new context specific MBCO is used for enrichment analysis of the input gene list via Fisher's Exact Test. Results are ranked by p-value and the top 3 level-2 or top 5 level-3 predictions (that are either SCPs or SCP-unions) are connected with each other based on all MBCO horizontal interactions to generate SCP-networks. See (Hansen et al. 2017) for details.

Significantly, up- or down-regulated genes with a with a minimum $\log_2$ fold change of $\pm \log_2(1.3)$ were subjected to standard enrichment analysis using MBCO and Fisher's Exact Test. All SCPs with a nominal significance of at least 5% at a particular time point were considered as significant and investigated for biological relevance.

siRNA testing in neurite outgrowth assay

Briefly, primary cortical neurons were seeded on one side of micro fluidity chambers. The two sites of the chambers are separated by a 150 µm microgroove sidewall that contains slits that are too small for whole cells to pass, but large enough to allow neurite growth into the other side of the chamber. Consequently, neurites will grow across the neurite site, allowing an easy quantification of outgrowth length. After transfection we waited for 48h to allow degradation of residual proteins. Basal outgrowth not attributable to the siRNAs was removed by axotonomy. Experiments were stopped, cells and neurites stained with anti-βIII tubulin (Tuj1; Covance). To quantify NOG we imaged the slides on a LSM880 confocal microscope (10x or 20x, zoom ins: 31x or 63x). For details, see (Yadaw et al. 2017).

Computational analysis of neurite outgrowth

We used the Image J software and the Plot Profile function to analyze neurite outgrowth, starting at the edge of the microgroove. This function calculates the average intensity of all pixels at a certain distance from the microgroove. In case of multiple images of one micro fluidity chamber, we calculated the average intensity for each image (without double quantification of overlapping areas in the images) and generated the average intensities for the whole chamber by combining

the intensities of the individual images (under consideration of quantified image sizes). Each experiment contained one to three controls. In case of multiple controls we calculated the mean average intensities that were used for any further analyses. To allow comparison of the results across different experiments, we normalized all average intensities of each siRNA or control of one experiment towards control average expression at 100 μm. We subtracted the normalized control average intensities from the average intensities of each siRNA treatment to analyze the effect of each siRNA on NOG. Negative differences indicate that the knock down of the corresponding gene inhibits NOG, positive differences indicate that the knock down stimulates NOG.

Figure 1A

HU210 induced gene expression

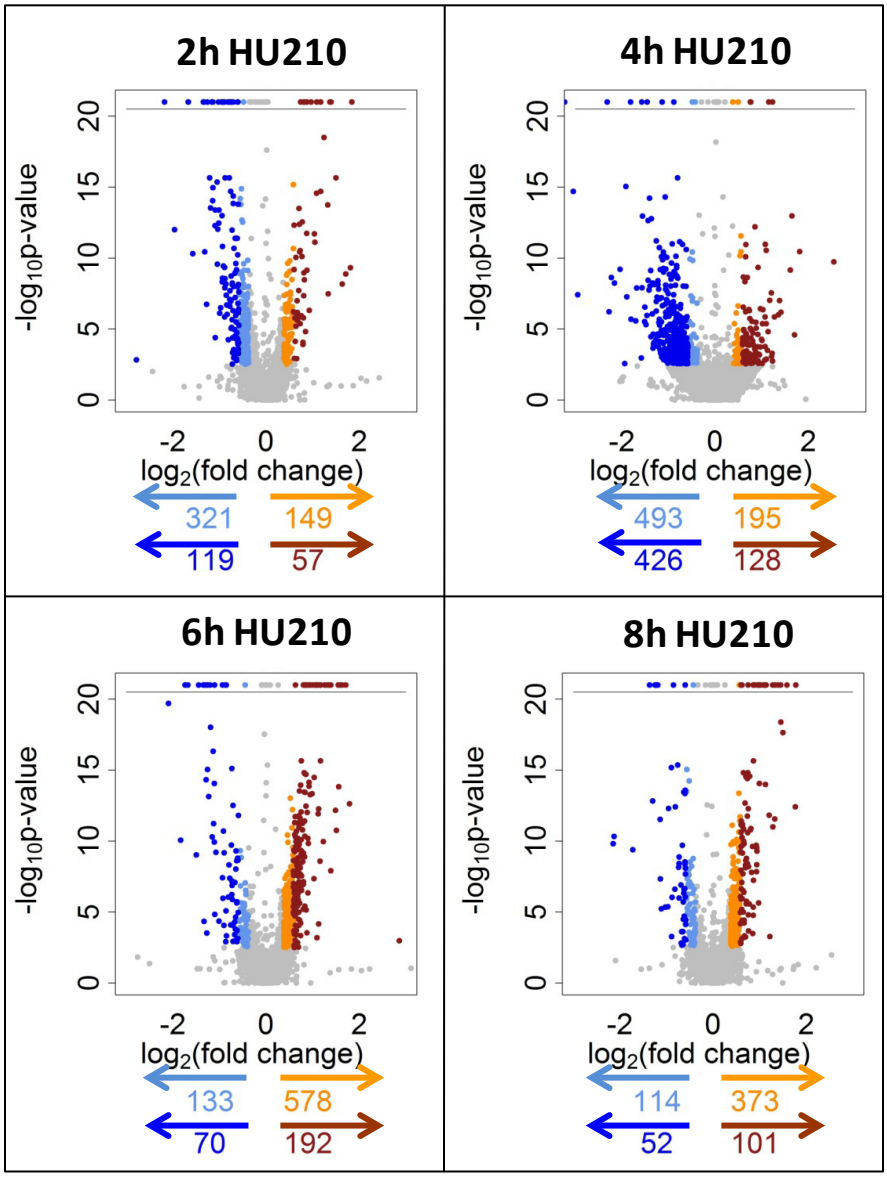

Figure 1B

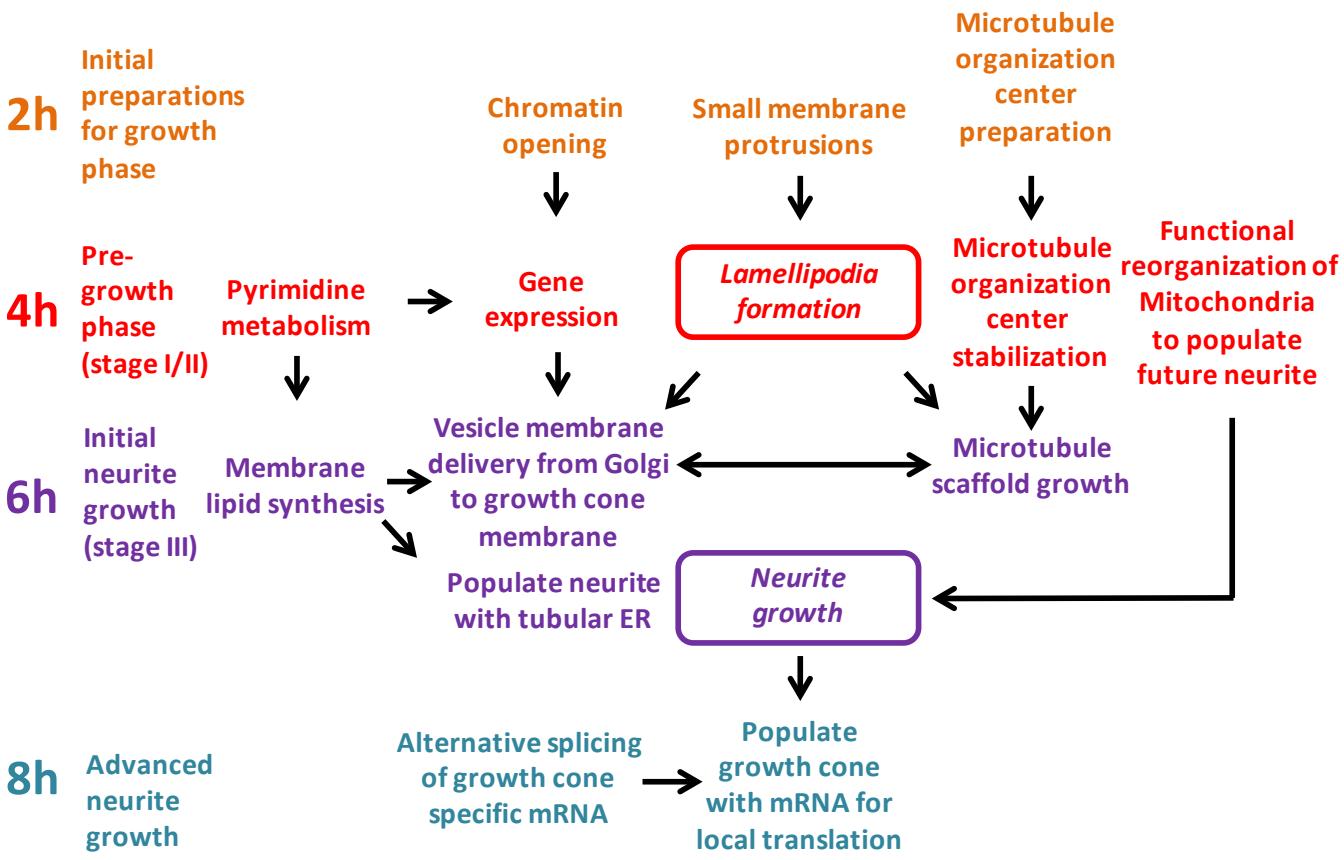
2h
Initial preparations for growth phase
Chromatin opening
Small membrane protrusions
Microtubule organization center preparation
4h
Pre-growth phase (stage I/II)
Pyrimidine metabolism
Gene expression
Lamellipodia formation
Microtubule organization center stabilization
Functional reorganization of Mitochondria to populate future neurite
6h
Initial neurite growth (stage III)
Membrane lipid synthesis
Vesicle membrane delivery from Golgi to growth cone membrane
Microtubule scaffold growth
Populate neurite with tubular ER
Neurite growth
8h
Advanced neurite growth
Alternative splicing of growth cone specific mRNA
Populate growth cone with mRNA for local translation

Figure 1C

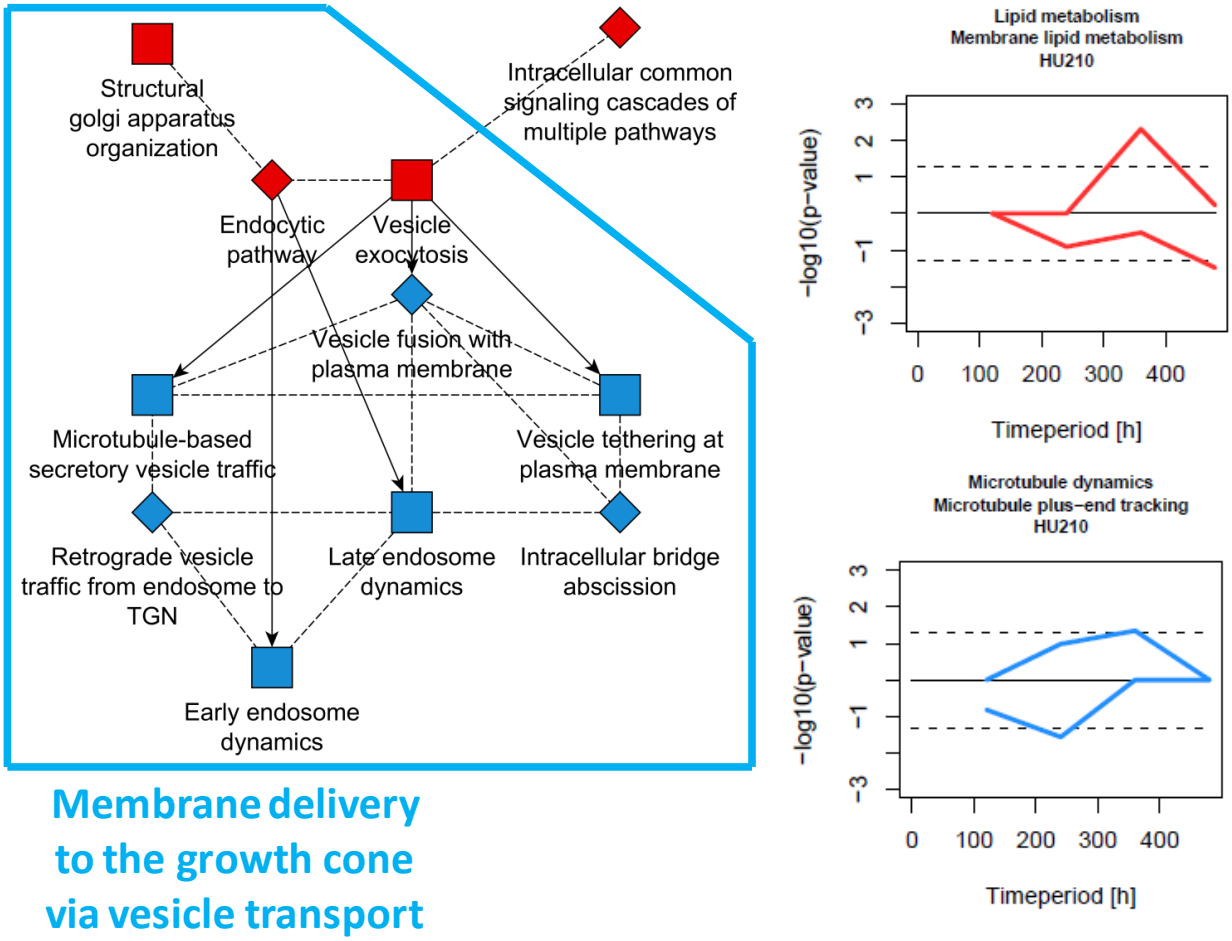

Figure 1: Chronological activation of distributed interdependent SCPs during neurite outgrowth (NOG) matches their dependencies. (A) Neuro2A cells were stimulated with the Cb1R agonist HU210 for indicated time periods, followed by identification of differentially expressed genes (DEGs). Volcano plots show DEGs (orange/light blue: FDR 5% and a minimum fold change of +/- $\log_2(1.3)$, red/dark blue: FDR 5% and a minimum fold change of +/- $\log_2(1.5)$). (B) DEGs were subjected to standard and dynamic enrichment analysis using the Molecular Biology of the Cell Ontology (MBCO) to characterize sub-cellular processes (SCPs) and SCP-networks that are involved in NOG. Predicted SCPs describe multiple sub-cellular functions that are activated in a chronological order that matches their dependencies. Framed SCPs describe functions that can be associated with morphological changes at neurite outgrowth

stages I and III. (C) Example SCP-networks and SCPs that were predicted based on up-regulated genes after 6h HU210. Dynamic enrichment analysis identified level-2 and level-3 networks that both describe microtubule vesicle trafficking between the TGN, endosomes and plasma membrane, suggesting that after 6h HU210 the cellular synthesis focuses on proteins involved in membrane delivery from the TGN to the growth cone. Concordantly, standard enrichment analysis predicts the up-regulation of transcripts involved in membrane lipid metabolism and microtubule plus-end-tracking. The SCP-network also contains an SCP that describes retrograde vesicle traffic from the endosome to the TGN (framed). Left panel: red nodes: level-2 SCPs, Blue nodes: level-3 SCPs, arrows: hierarchical relationships between parent and child SCPs, dashed lines: horizontal relationships between SCPs of the same level. The predicted unconnected SCP 'Classical complement pathway' was removed from the network. Right panel: Minus $\log_{10}$(p-values) for the indicated SCPs based on up-regulated genes (above 0) and down-regulated genes (below 0) of the indicated timepoints. Dashed lines indicate nominal significance (alpha = 0.05). Colors indicate SCP level as on the left panel. See suppl. figure 1 and 2 for complete standard and dynamic enrichment results.

Table 1

Sub-cellular function	NCBI symbol	Is differentially expressed gene (DEG)?	NCIB description
Exosome complex mediated RNA degradation	DIS3	No DEG	DIS3 homolog, exosome endoribonuclease and 3'-5' exoribonuclease
mRNA splicing	MBNL1	No DEG	muscleblind like splicing factor 1
mRNA splicing	SF3A2	No DEG	splicing factor 3a, subunit 2
mRNA splicing	SNRNP70	No DEG	small nuclear ribonucleoprotein 70 (U1)
Pyrimidine de-novo synthesis	CAD	No DEG	carbamoyl-phosphate synthetase 2, aspartate transcarbamylase, and dihydroorotase
Pyrimidine de-novo synthesis	DHODH	Up-regulated at 4h	dihydroorotate dehydrogenase
Pyrimidine salvage	TYMP	Up-regulated at 4h	thymidine phosphorylase
Synthesis of complex gangliosides	PLEKHA8	No DEG	pleckstrin homology domain containing, family A (phosphoinositide binding specific) member 8
Synthesis of complex gangliosides	UGCG	Down-regulated at 2h, Up-regulated at 6h and 8h	UDP-glucose ceramide glucosyltransferase
Sphingomyeline synthesis	COL4A3BP	No DEG	collagen, type IV, alpha 3 (Goodpasture antigen) binding protein
Phosphatidylcholine (PC) synthesis	PCYT1A	No DEG	phosphate cytidylyltransferase 1, choline, alpha isoform
Phosphatidylethanolamine (PE) synthesis	PCYT2	No DEG	phosphate cytidylyltransferase 2, ethanolamine
Mitochondrial transport	RHOT1	Down-regulated at 4h	ras homolog family member T1
Mitochondrial fusion	MFN2	No DEG	mitofusin 2
Mitochondrial translation	TUFM	No DEG	Tu translation elongation factor, mitochondrial
Mitochondrial protein import	MTX1	Down-regulated at 6h	metaxin 1

Table 1

Sub-cellular function	NCBI symbol	Is differentially expressed gene (DEG)?	NCIB description
Golgi derived vesicle loading on microtubules, Actin-microtubule crosslinking	MACF1	Down-regulated at 4h, Up-regulated at 6h	microtubule-actin crosslinking factor 1
Integrin internalization and recycling	RAB21	Up-regulated at 6h and 8h	RAB21, member RAS oncogene family
Vesicle priming during exocytosis	UNC13B	No DEG	unc-13 homolog B
Exocyst mediated vesicle tethering during exocytosis	EXOC4	No DEG	exocyst complex component 4
Exocyst mediated vesicle tethering during exocytosis	EXOC7	No DEG	exocyst complex component 7
Retromer mediated endosomal sorting	SNX2	No DEG	sorting nexin 2
Retromer mediated endosomal sorting	VPS35	No DEG	VPS35 retromer complex component
Cytokinesis/Neurite pruning/Multivesicular body formation	CHMP6	No DEG	charged multivesicular body protein 6
Multivesicular body formation	HGS	No DEG	HGF-regulated tyrosine kinase substrate
Cytokinesis/Neurite pruning/Multivesicular body formation	TSG101	No DEG	tumor susceptibility gene 101
Tubular endoplasmic reticulum formation	ATL2	No DEG	atlastin GTPase 2
Tubular endoplasmic reticulum formation	RTN1	No DEG	reticulon 1
Complement activation	MASP2	Down-regulated at 4h and 6h	mannan-binding lectin serine peptidase 2
Copper transmembrane transport	ATP7B	No DEG	ATPase, Cu++ transporting, beta polypeptide
Protein glycosylation	MAN1A2	Up-regulated at 6h	mannosidase, alpha, class 1A, member 2
Synthesis of non-ATP Nucleoside triphosphates	NME1	Up-regulated at 2h and 4h	NME/NM23 nucleoside diphosphate kinase 1
Nuclear protein translocation	NUP88	Up-regulated at 8h	nucleoporin 88

Table 1: Selected genes for siRNA knock down screening. We selected representative genes for the indicated sub-cellular functions to test the effect of their knock down on neurite outgrowth. Most of the selected genes were not among the differentially expressed genes (No DEG) after HU210 treatment of N2A cells.

Figure 2A

Scrambl transfected Primary neurons

Primary neurons transfected with siRNA against Tufm

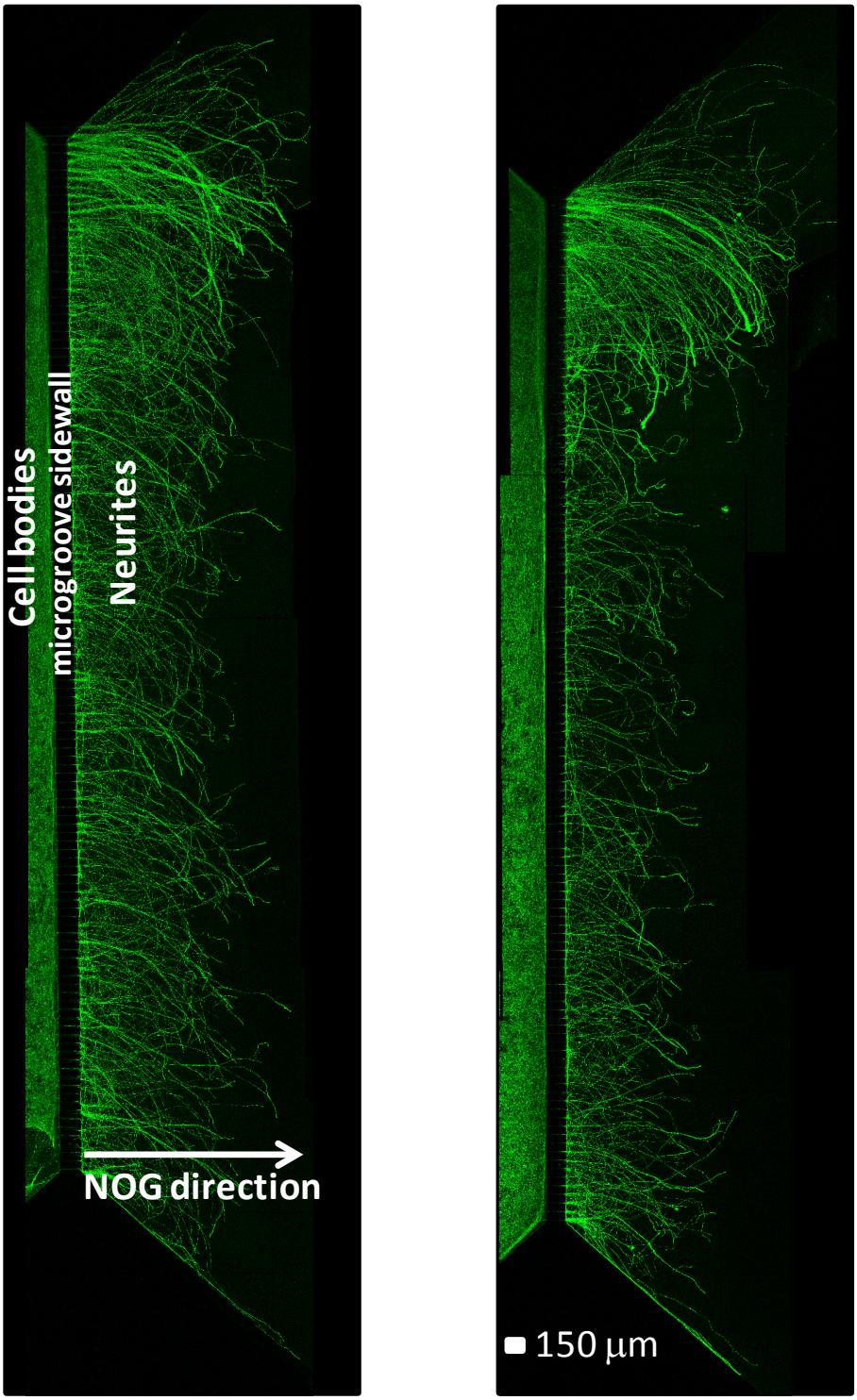

Figure 2B

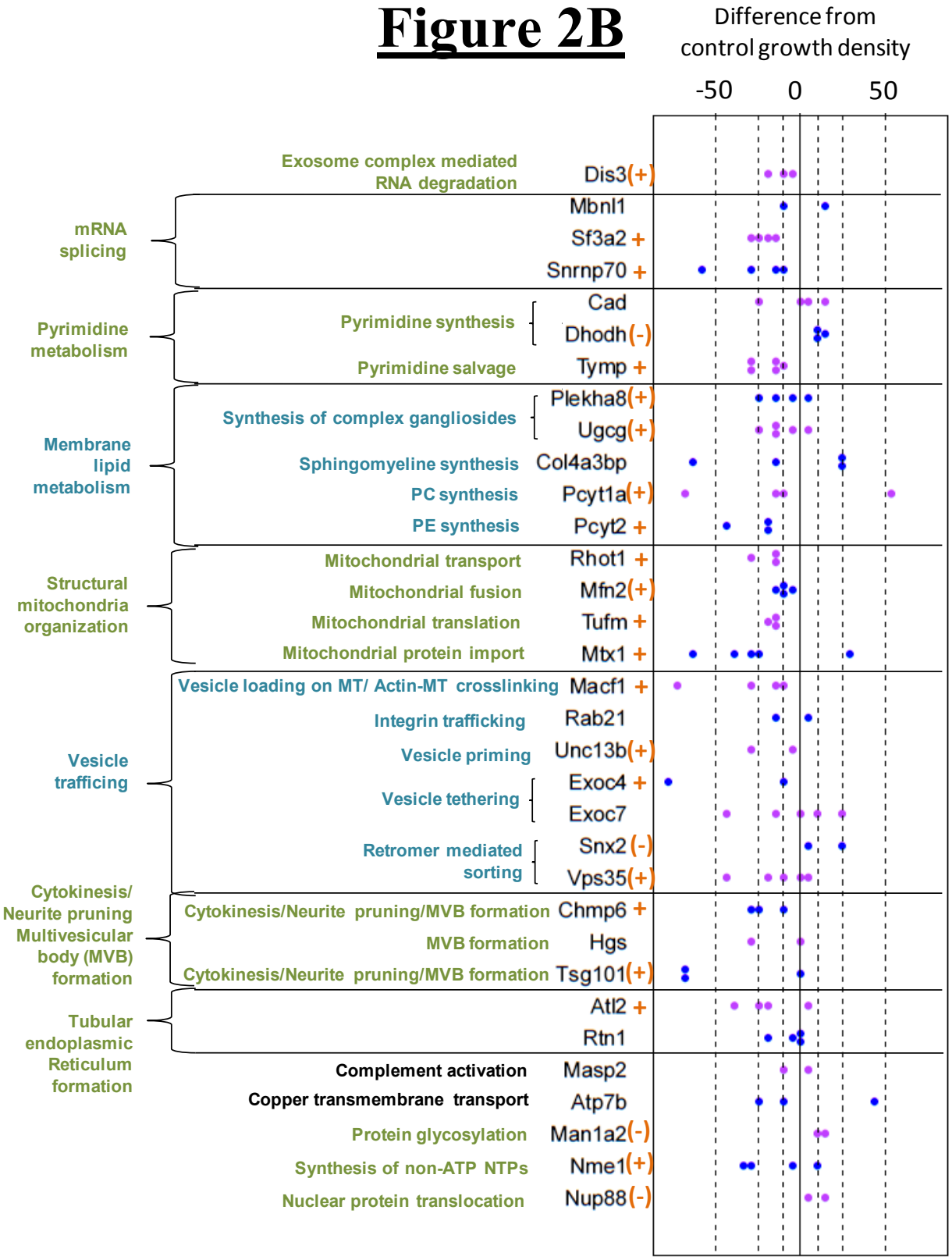
Difference from control growth density
-50
0
50
Exosome complex mediated RNA degradation
Dis3(+)
mRNA splicing
Mbnl1
Sf3a2 +
Snrnp70 +
Pyrimidine metabolism
Pyrimidine synthesis
Cad
Dhodh(-)
Pyrimidine salvage
Tymp +
Membrane lipid metabolism
Synthesis of complex gangliosides
Plekha8(+)
Ugcg(+)
Sphingomyeline synthesis
Col4a3bp
PC synthesis
Pcyt1a(+)
PE synthesis
Pcyt2 +
Structural mitochondria organization
Mitochondrial transport
Rhot1 +
Mitochondrial fusion
Mfn2(+)
Mitochondrial translation
Tufm +
Mitochondrial protein import
Mtx1 +
Vesicle trafficing
Vesicle loading on MT/ Actin-MT crosslinking
Macf1 +
Integrin trafficking
Rab21
Vesicle priming
Unc13b(+)
Vesicle tethering
Exoc4 +
Exoc7
Retromer mediated sorting
Snx2 (-)
Vps35(+)
Cytokinesis/ Neurite pruning Multivesicular body (MVB) formation
Cytokinesis/Neurite pruning/MVB formation
Chmp6 +
MVB formation
Hgs
Cytokinesis/Neurite pruning/MVB formation
Tsg101(+)
Tubular endoplasmic Reticulum formation
Atl2 +
Rtn1
Complement activation
Masp2
Copper transmembrane transport
Atp7b
Protein glycosylation
Man1a2(-)
Synthesis of non-ATP NTPs
Nme1(+)
Nuclear protein translocation
Nup88(-)

Figure 2: siRNA knock down experiments document involvement of multiple SCPs. (A) P1 rat cortical neurons were transfected with siRNA against selected representative pathway genes (shown: Tufm) or scrambled siRNAs. Neurites and cell bodies were stained for β-III tubulin to document neurite outgrowth. (B) Neurite outgrowth fluorescence intensities were quantified and the average intensity at each distance from the microgroove sidewall calculated. All intensities of one experiment were normalized towards control average intensity at 100 μm. Differences in the normalized average intensity at 750 μm between siRNA transfected and control cells were calculated and visualized. Negative differences indicate less neurite outgrowth after siRNA knock down. Genes whose knock down inhibited NOG or showed a tendency to inhibit NOG are labeled with '+' or '(+)', respectively, since they are positive regulators. Similarly, genes whose knock down increased or showed the tendency to increase NOG are labeled with '-' or '(-)', since they are negative regulators of NOG. Each dot represents an independent experiment that tested the effect of the knock down of the indicated gene. Dot colors alternate between adjacent genes for visualization purposes. Corresponding SCPs are colored in blue, if they can be directly associated with neurite shaft growth and in green, if they describe deep more basal regulatory functions. Black SCPs summarize genes that did not show an effect on neurite outgrowth at 750 μm.

Figure 3A

Pyrimidine metabolism

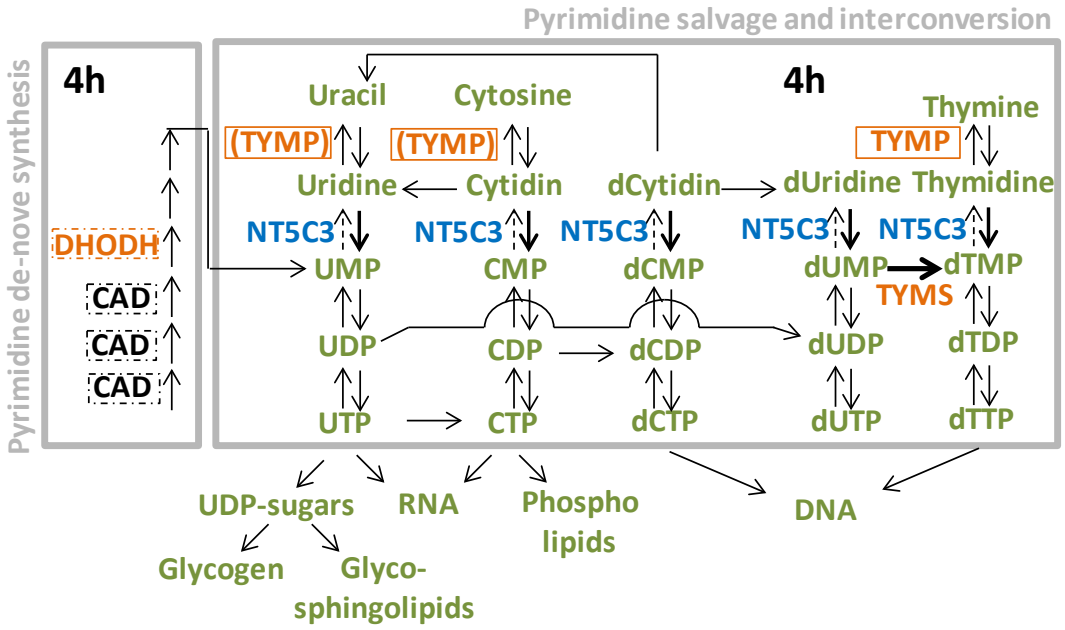

Figure 3B

Membrane lipid metabolism

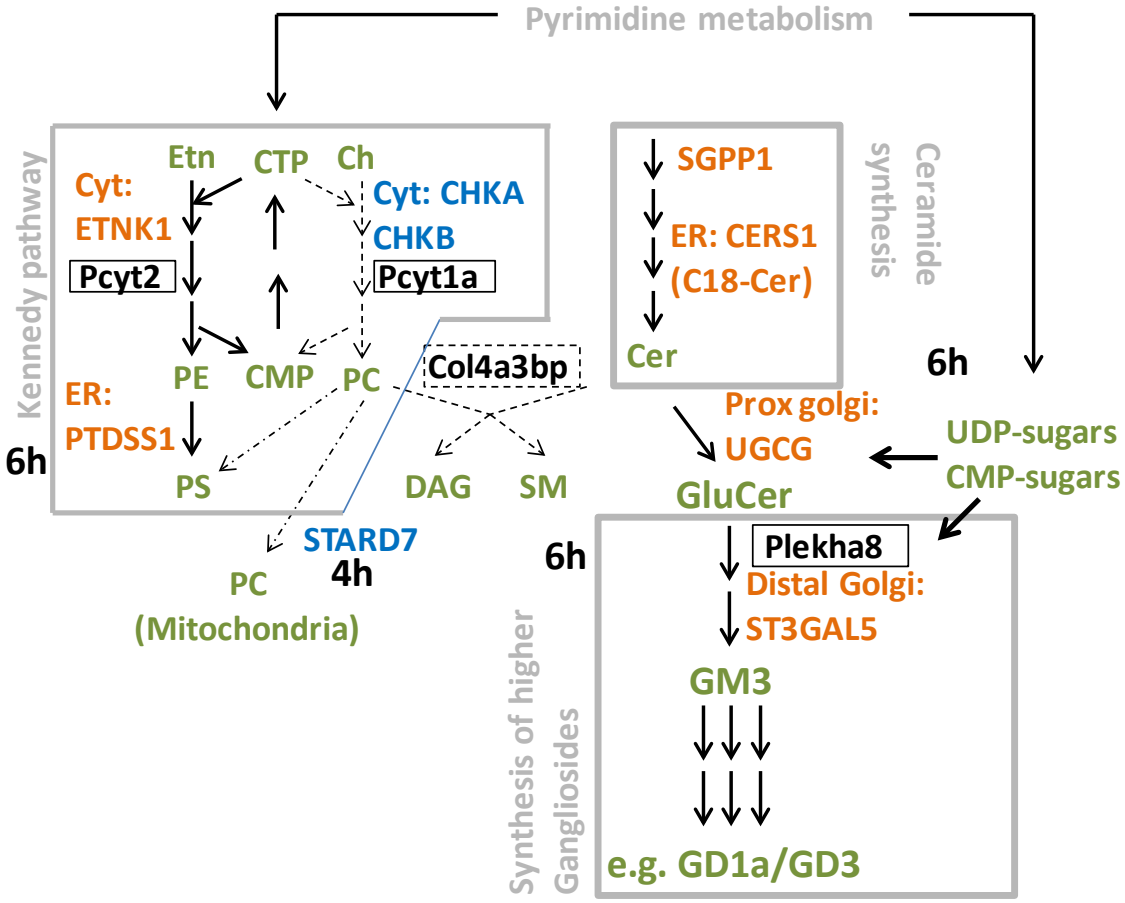

Figure 3C

Structural mitochondria organization

4h

Mitochondrial transport

retrograde → anterograde

RHOT2

RHOT1

Mitochondrial fusion and fission

fission → fusion

MARCH5, MFF

MFN2

Mitochondrial protein import and folding

Protein import IMM

TIMM44

Mtx1

Import signal removal

IMMP2L

folding

HSPD1,HSPE1

Mitochondrial gene expression

mitochondrial transcription

TFAM

mitochondrial ribosomes

MRPLI3, MALSU1

mitochondrial translation

MTIF3

mitochondrial translation

Tufm

mitochondrial tRNA activation

TRMU, VARS2, GTPBP3

LARS, OSGEPL1

Mitochondrial Calcium uptake

MICU3

Mitochondrial oxidative phosphorylation

NDUFB3, COX7C

COX7B, COX5A, ADCK3, NUDFA5, COQ10B,TTC19

Outer membrane dynamics

SH3GLB1

Mitochondrial iron-sulfur (Fe-S) cluster assembly

BOLA1

Figure 3D

Cytosolic mRNA degradation

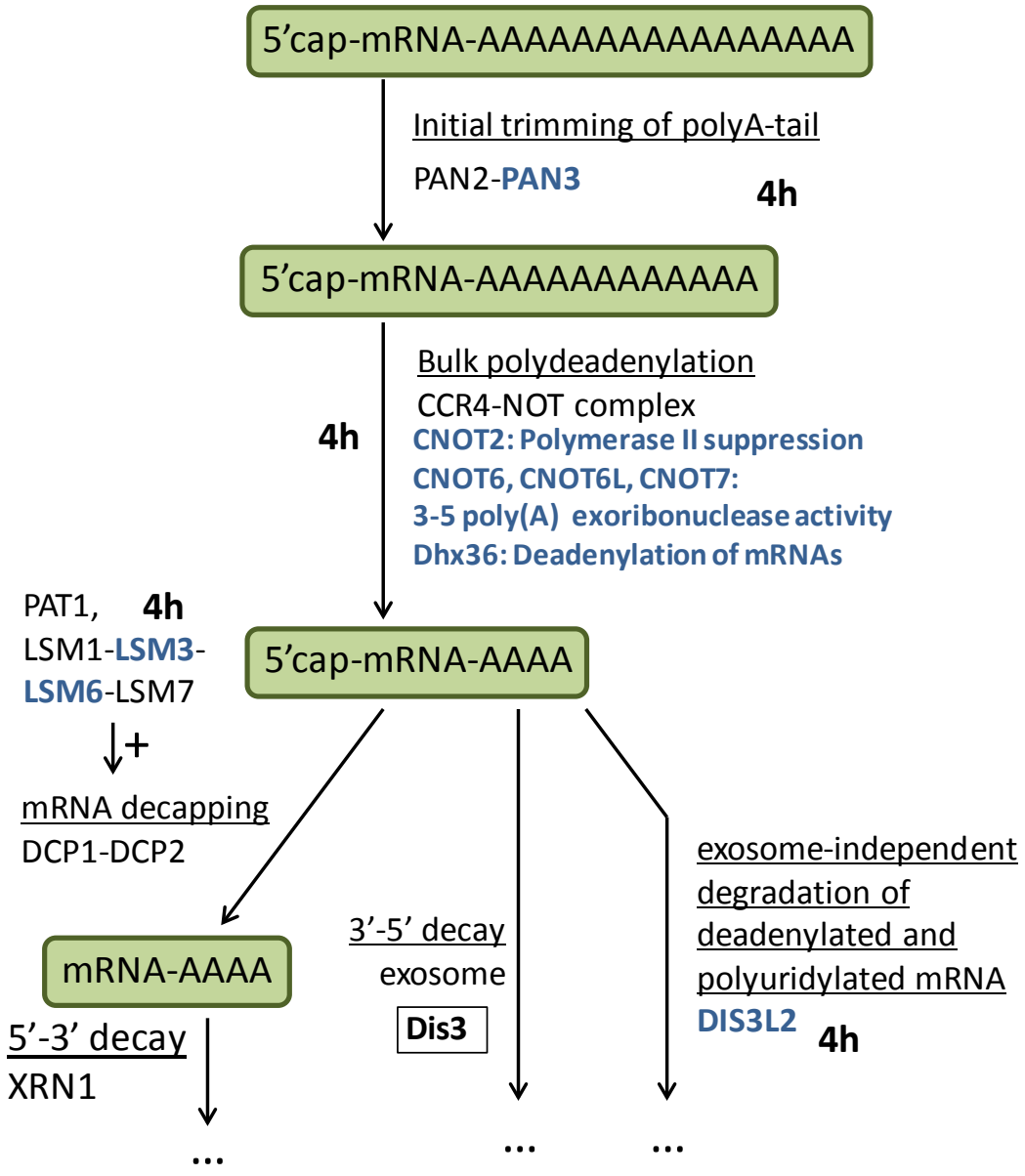

Figure 3E

Vesicle transport between TGN and growth cone

SCPs involved in anterograde vesicle movement from the TGN to the growth cone

Golgi vesicle transport:
6h: Ap1a1, Ap1s2, Ap3s1, Gga3, Tmed2, Rab10, Sgsm2, Bcap29, Rab6a, Golph3
8h: Ap3s1, Ap4s1, Golph3, Rab10, Tmed2, Bcap29, Rab6a
Plekha8

Microtubule based anterograde vesicle transport
6h: Ap3s1, Fyco1, Rab6a, Rab21, Snapin
8h: Ap3s1, Rab6a, Rab21
Macf1

Exocytosis:
6h: Snapin, Rala, Exoc5, Rab21, Rab2b, Rab5a, Tmem79
8h: Doc2a, Exoc1, Rab21, Tbc1d12 Vamp2, Exoc5, Dysf
Unc13b, Exoc4, Exoc7

SCPs involved in retrograde vesicle movement from the TGN to the growth cone

Retrograde transport from endocytic pathway to Golgi
6h: Snx3, Rab9, Rab6a, Sgsm2, Pafah1b1
8h: Rab43, Rab6a, Snx3
Vps35, Snx2

Multivesicular body genesis
Chmp6, Hgs, Tsg101

Endosome dynamics
6h: Rab5a, Stx7, Snx10
8h: Rab5a, Ehd4

Endosomal to lysosome transport
6h: Fyco1, Rab12, Rab21, Rnf115, Snapin
8h: Hook3, Rab21, Rnf115

Endocytosis
6h: Snx18, Rala, Fcho1, WASL, Snapin, Synj2bp, Dnm3
8h: Arf6, Hip1r, Fcho1

Recycling from endosome to plasma membrane
6h: Snx3, Linc7c, Micall2, Spast, Rab21
8h: Snx3, Rab21
Vps35, Snx2

Figure 3: Enzymatic reactions involved in pyrimidine and membrane lipid metabolism. (A) Enzymatic reactions involved in pyrimidine de-novo synthesis and pyrimidine salvage and interconversion (adopted from (Garavito et al. 2015) under consideration of (Vincenzetti et al. 2016). Up- (orange) and down-regulated (blue) genes suggest a net flux of pyrimidine metabolites to pyrimidines that can be used to generate complex molecules. siRNA knock down results suggest the dependence of NOG on pyrimidine salvage, but not of pyrimidine de novo synthesis. Orange/blue: up-/down-regulated genes (based on a mininum $\log_2$(fold change) of +/- $\log_2$(1.3)). Green: metabolites. Genes surrounded by solid rectangles: siRNA targets with an effect on NOG. Genes surrounded by dashed rectangles: siRNA targets with no effect on NOG. (B) Enzymatic reactions and transport proteins involved in phospholipid, ceramide and ganglioside synthesis. Up- and down regulated genes as well as siRNA knock down results suggest a shift of phospholipid production from PC to PE/PS and an increase in ganglioside production. Etn: Ethanolamine, Ch: Choline, PE: Phosphatidylethanolamine, PS: Phosphatidylserin, PC: Phosphatidylcholine, Cer: Ceramide GM3/GD1a/GD3: GM3/GD1a/GD3 ganglioside, GluCer: Glucosylceramide, SM: Sphingomyeline, DAG: Diacylglycerol (C) Up- and down-regulated genes and siRNA targets involved in Structural mitochondria organization. (D) Up- and down-regulated genes in cytosolic mRNA degradation (Norbury 2013). (E) Up- and down-regulated genes in vesicle transport between TGN and growth cone.

Figure 4A

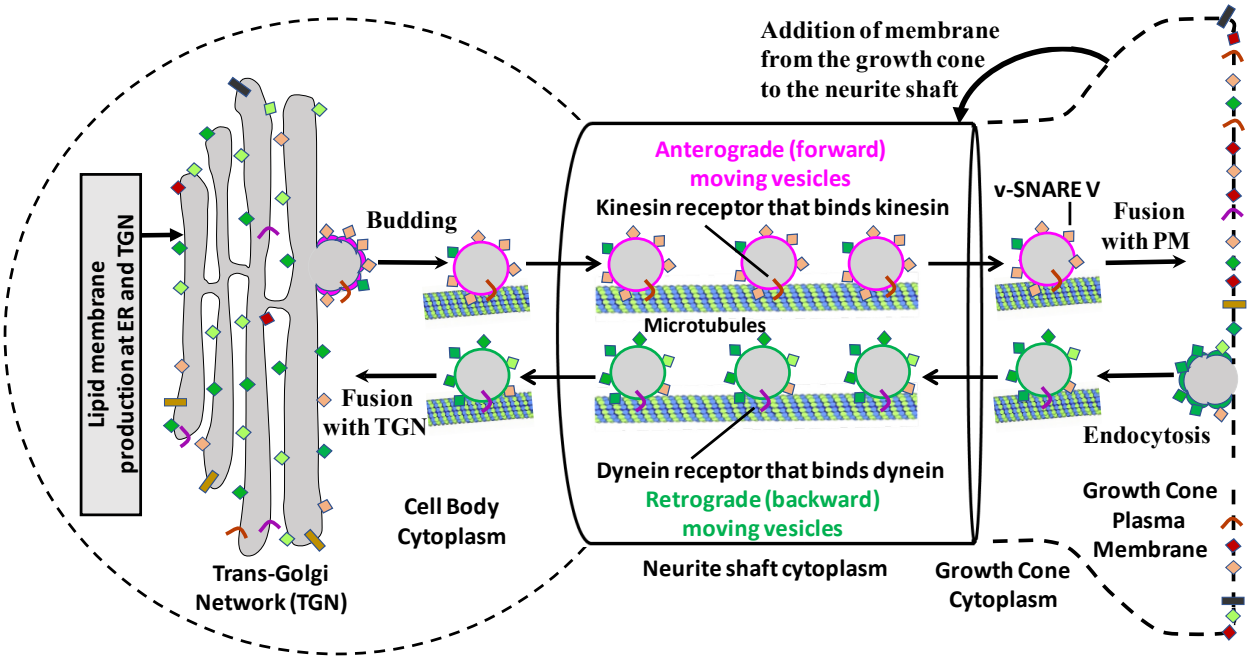

Figure 4B

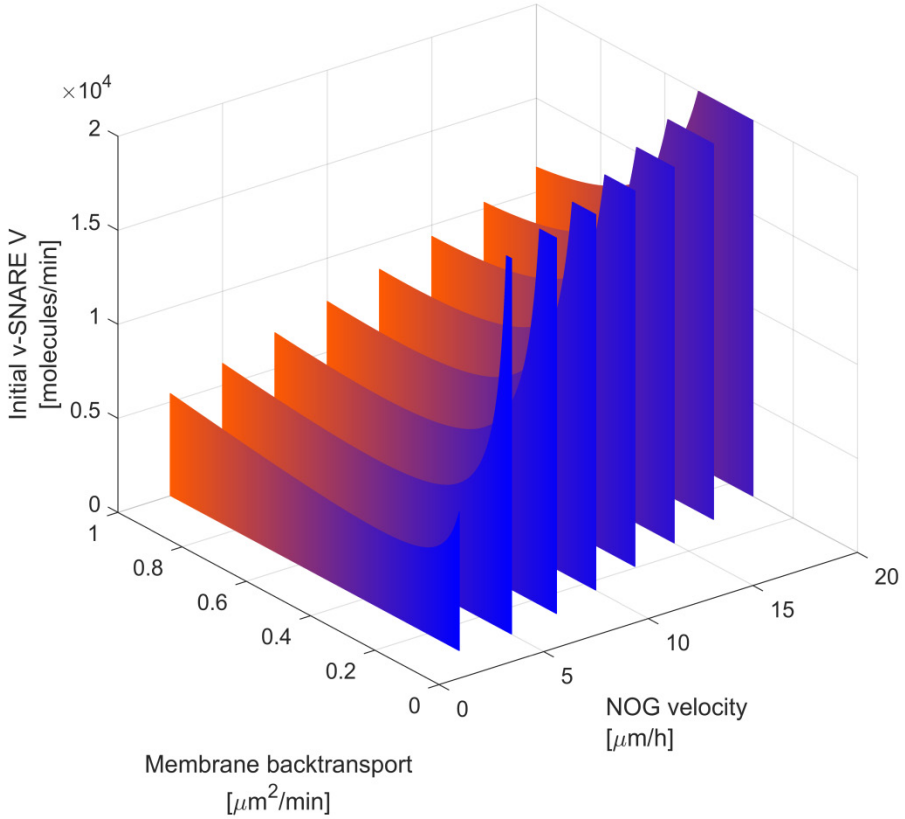

Figure 4C

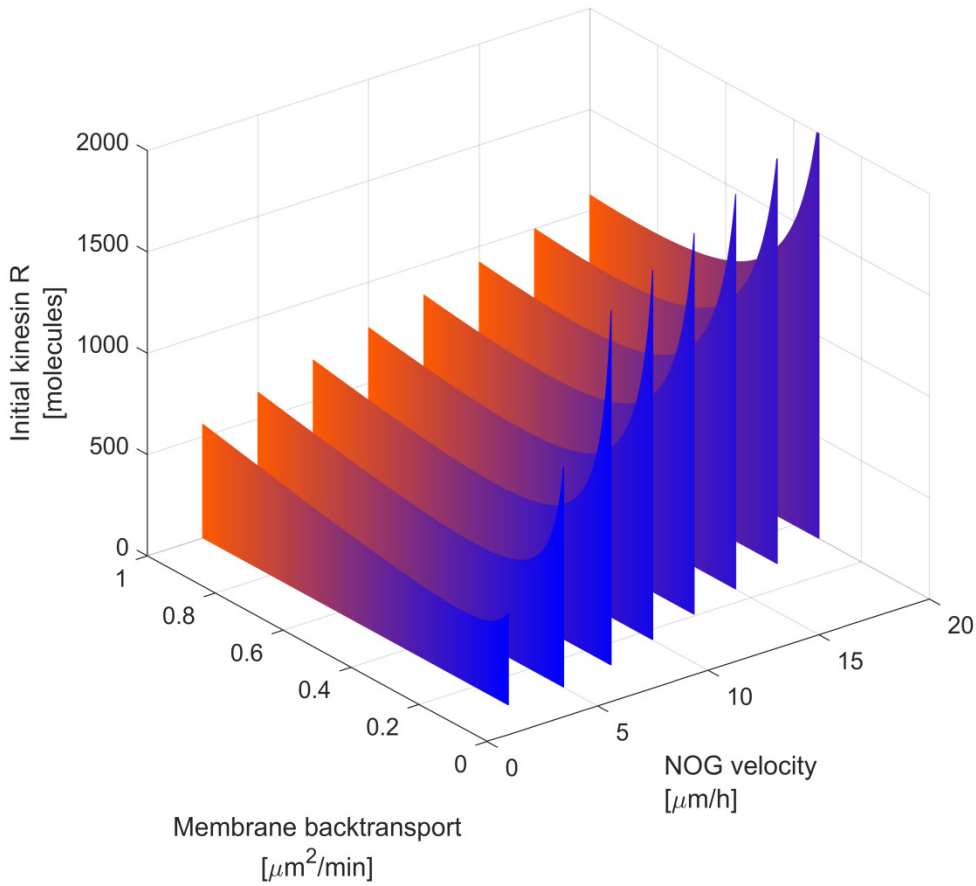

Figure 4: Dynamic model of vesicular transport predicts that increase in vesicle backtransport is necessary for sufficient back transport of v-SNAREs and kinesin receptors from the growth cone to the TGN. (A) We used our compartmental ODE model that simulates membrane production, vesicle membrane transport to the growth cone and microtubule growth to analyze how membrane back transport influences NOG (See text for details). Part of our NOG model is an analytical solution that predicts kinetic parameter sets that allow NOG growth under a certain velocity without violation of SCP model constraints. Figure adopted from (Yadaw et al. 2017). (B/C) Our analytical solution predicts that for each velocity there is a threshold for the membrane back transport rate below which the amount of v-SNAREs (B) and kinesin receptors (C) rapidly increase. Below a second threshold NOG is not possible anymore without violation of the model constraints (missing entries on the right side of each wall). Both thresholds shift to higher rates with increasing NOG velocity. Such constellations are the consequence of the limited amount of binding spots for SNAREs and kinesin receptors on backward moving vesicles. The more forward moving vesicles bring membrane from the TGN to the growth cone, the more v-SNAREs and kinesin receptors need to be brought back from the growth cone to the TGN to be available for the next set of forward moving vesicles.

Consequently, the amount of backward moving vesicles has to be increased accordingly. (One of our model constraints postulates that 90% of anterograde vesicles are part of a stationary vesicle reservoir within the neurite shaft. Consequently, the increasing neurite shaft acts as a sink for antereograde vesicles and their membrane proteins components. Such loss of v-SNAREs and kinesin receptors needs to be compensated by de-novo production of new proteins, increasing the total amount of v-SNAREs and kinesin receptors. Shown are the initial v-SNARE and kinesin receptor counts, before the neurite starts growing.)

Figure 5

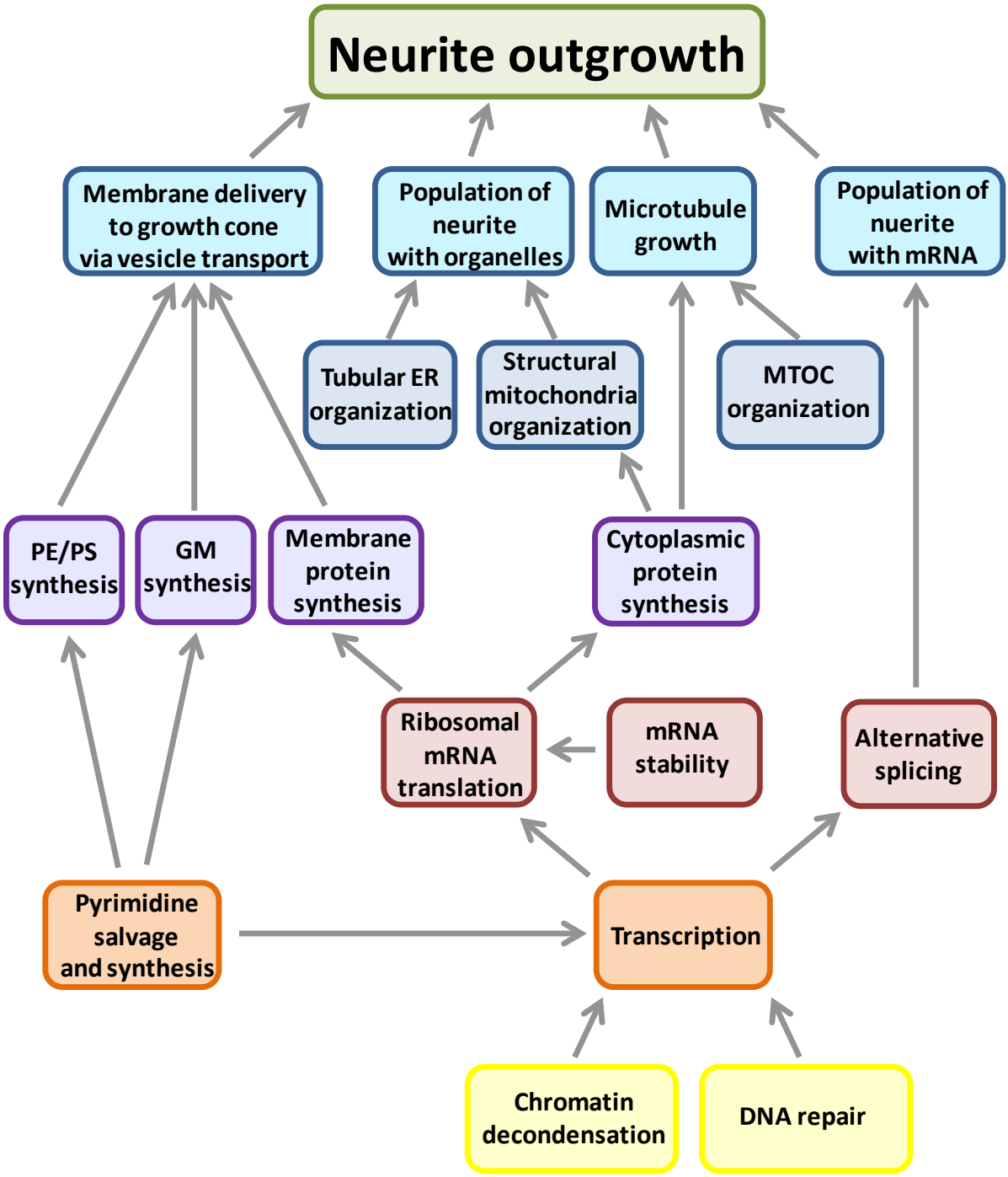
Neurite outgrowth
Membrane delivery to growth cone via vesicle transport
Population of neurite with organelles
Microtubule growth
Population of nuerite with mRNA
Tubular ER organization
Structural mitochondria organization
MTOC organization
PE/PS synthesis
GM synthesis
Membrane protein synthesis
Cytoplasmic protein synthesis
Ribosomal mRNA translation
mRNA stability
Alternative splicing
Pyrimidine salvage and synthesis
Transcription
Chromatin decondensation
DNA repair

Figure 5: Neurite outgrowth depends on deep and distributed regulation. Multiple SCPs interact with each other to enable neurite outgrowth. The SCPs describe sub-cellular functions that can either be directly associated with neurite shaft and neurite scaffold growth, e.g. Membrane lipid delivery to the growth cone and Microtubule growth, or describe deeper more basal sub-cellular functions, e.g. Pyrimidine salvage and synthesis. The network proposes SCP interactions that constitute the deep and distributed regulation of NOG.

References

Alberts, B., A. Johnson, J. Lewis, D. Morgan, M. Raff, K. Roberts & P. Walter. 2015. *Molecular Biology of the Cell*. Garland Science, Taylor & Francis Group.

Arimura, N. & K. Kaibuchi (2007) Neuronal polarity: from extracellular signals to intracellular mechanisms. *Nat Rev Neurosci,* 8**,** 194-205.

Berg, J. M., J. L. Tymoczko & L. Stryer. 2002. *Biochemistry*. New York: W. H. Freeman.

Blusztajn, J. K., M. Liscovitch, C. Mauron, U. I. Richardson & R. J. Wurtman (1987a) Phosphatidylcholine as a precursor of choline for acetylcholine synthesis. *J Neural Transm Suppl,* 24**,** 247-59.

Blusztajn, J. K., M. Liscovitch & U. I. Richardson (1987b) Synthesis of acetylcholine from choline derived from phosphatidylcholine in a human neuronal cell line. *Proc Natl Acad Sci U S A,* 84**,** 5474-7.

Bradke, F. & C. G. Dotti (1997) Neuronal polarity: vectorial cytoplasmic flow precedes axon formation. *Neuron,* 19**,** 1175-86.

Bradke, F., J. W. Fawcett & M. E. Spira (2012) Assembly of a new growth cone after axotomy: the precursor to axon regeneration. *Nat Rev Neurosci,* 13**,** 183-93.

Bromberg, K. D., A. Ma'ayan, S. R. Neves & R. Iyengar (2008) Design logic of a cannabinoid receptor signaling network that triggers neurite outgrowth. *Science,* 320**,** 903-9.

Burgo, A., V. Proux-Gillardeaux, E. Sotirakis, P. Bun, A. Casano, A. Verraes, R. K. Liem, E. Formstecher, M. Coppey-Moisan & T. Galli (2012) A molecular network for the transport of the TI-VAMP/VAMP7 vesicles from cell center to periphery. *Dev Cell,* 23**,** 166-80.

Carter, J. M., L. Demizieux, R. B. Campenot, D. E. Vance & J. E. Vance (2008) Phosphatidylcholine biosynthesis via CTP:phosphocholine cytidylyltransferase 2 facilitates neurite outgrowth and branching. *J Biol Chem,* 283**,** 202-12.

Cheng, A., Y. Hou & M. P. Mattson (2010) Mitochondria and neuroplasticity. *ASN Neuro,* 2**,** e00045.

Chisholm, A. D., H. Hutter, Y. Jin & W. G. Wadsworth (2016) The Genetics of Axon Guidance and Axon Regeneration in Caenorhabditis elegans. *Genetics,* 204**,** 849-882.

Collart, M. A. (2016) The Ccr4-Not complex is a key regulator of eukaryotic gene expression. *Wiley Interdiscip Rev RNA,* 7**,** 438-54.

Crutcher, K. A. (1986) The role of growth factors in neuronal development and plasticity. *CRC Crit Rev Clin Neurobiol,* 2**,** 297-333.

D'Angelo, G., E. Polishchuk, G. Di Tullio, M. Santoro, A. Di Campli, A. Godi, G. West, J. Bielawski, C. C. Chuang, A. C. van der Spoel, F. M. Platt, Y. A. Hannun, R. Polishchuk, P. Mattjus & M. A. De

Matteis (2007) Glycosphingolipid synthesis requires FAPP2 transfer of glucosylceramide. *Nature,* 449**,** 62-7.

Daniotti, J. L. & R. Iglesias-Bartolomé (2011) Metabolic pathways and intracellular trafficking of gangliosides. *IUBMB Life,* 63**,** 513-20.

De Almeida, C., H. Scheer, H. Zuber & D. Gagliardi (2018) RNA uridylation: a key posttranscriptional modification shaping the coding and noncoding transcriptome. *Wiley Interdiscip Rev RNA,* 9.

de Anda, F. C., K. Meletis, X. Ge, D. Rei & L. H. Tsai (2010) Centrosome motility is essential for initial axon formation in the neocortex. *J Neurosci,* 30**,** 10391-406.

Doidge, R., S. Mittal, A. Aslam & G. S. Winkler (2012) Deadenylation of cytoplasmic mRNA by the mammalian Ccr4-Not complex. *Biochem Soc Trans,* 40**,** 896-901.

Estrada-Bernal, A., S. D. Sanford, L. J. Sosa, G. C. Simon, K. C. Hansen & K. H. Pfenninger (2012) Functional complexity of the axonal growth cone: a proteomic analysis. *PLoS One,* 7**,** e31858.

Fadeel, B. & D. Xue (2009) The ins and outs of phospholipid asymmetry in the plasma membrane: roles in health and disease. *Crit Rev Biochem Mol Biol,* 44**,** 264-77.

Gallon, M. & P. J. Cullen (2015) Retromer and sorting nexins in endosomal sorting. *Biochem Soc Trans,* 43**,** 33-47.

Garavito, M. F., H. Y. Narváez-Ortiz & B. H. Zimmermann (2015) Pyrimidine Metabolism: Dynamic and Versatile Pathways in Pathogens and Cellular Development. *J Genet Genomics,* 42**,** 195-205.

Govek, E. E., S. E. Newey & L. Van Aelst (2005) The role of the Rho GTPases in neuronal development. *Genes Dev,* 19**,** 1-49.

Hanada, K., K. Kumagai, N. Tomishige & T. Yamaji (2009) CERT-mediated trafficking of ceramide. *Biochim Biophys Acta,* 1791**,** 684-91.

Hanada, K., K. Kumagai, S. Yasuda, Y. Miura, M. Kawano, M. Fukasawa & M. Nishijima (2003) Molecular machinery for non-vesicular trafficking of ceramide. *Nature,* 426**,** 803-9.

Hansen, J., D. Meretzky, S. Woldesenbet, G. Stolovitzky & R. Iyengar (2017) A flexible ontology for inference of emergent whole cell function from relationships between subcellular processes. *Sci Rep,* 7**,** 17689.

He, J. C., I. Gomes, T. Nguyen, G. Jayaram, P. T. Ram, L. A. Devi & R. Iyengar (2005) The G alpha(o/i)-coupled cannabinoid receptor-mediated neurite outgrowth involves Rap regulation of Src and Stat3. *J Biol Chem,* 280**,** 33426-34.

Higginbotham, H. R. & J. G. Gleeson (2007) The centrosome in neuronal development. *Trends Neurosci,* 30**,** 276-83.

Kilchert, C., S. Wittmann & L. Vasiljeva (2016) The regulation and functions of the nuclear RNA exosome complex. *Nat Rev Mol Cell Biol,* 17**,** 227-39.

Kim, E. & H. Jung (2015) Local protein synthesis in neuronal axons: why and how we study. *BMB Rep,* 48**,** 139-46.

Kozlowski, M. R., M. P. Rosser, E. Hall & A. Longden (1989) Effects of bradykinin on PC-12 cell differentiation. *Peptides,* 10**,** 1121-6.

Lannert, H., K. Gorgas, I. Meissner, F. T. Wieland & D. Jeckel (1998) Functional organization of the Golgi apparatus in glycosphingolipid biosynthesis. Lactosylceramide and subsequent glycosphingolipids are formed in the lumen of the late Golgi. *J Biol Chem,* 273**,** 2939-46.

Madabhushi, R., F. Gao, A. R. Pfenning, L. Pan, S. Yamakawa, J. Seo, R. Rueda, T. X. Phan, H. Yamakawa, P. C. Pao, R. T. Stott, E. Gjoneska, A. Nott, S. Cho, M. Kellis & L. H. Tsai (2015) Activity-Induced DNA Breaks Govern the Expression of Neuronal Early-Response Genes. *Cell,* 161**,** 1592-605.

Mattson, M. P. & J. Partin (1999) Evidence for mitochondrial control of neuronal polarity. *J Neurosci Res,* 56**,** 8-20.

Nakazawa, H., T. Sada, M. Toriyama, K. Tago, T. Sugiura, M. Fukuda & N. Inagaki (2012) Rab33a mediates anterograde vesicular transport for membrane exocytosis and axon outgrowth. *J Neurosci,* 32**,** 12712-25.

Norbury, C. J. (2013) Cytoplasmic RNA: a case of the tail wagging the dog. *Nat Rev Mol Cell Biol,* 14**,** 643-53.

Pfenninger, K. H. (2009) Plasma membrane expansion: a neuron's Herculean task. *Nat Rev Neurosci,* 10**,** 251-61.

Pooler, A. M., D. H. Guez, R. Benedictus & R. J. Wurtman (2005) Uridine enhances neurite outgrowth in nerve growth factor-differentiated PC12 [corrected]. *Neuroscience,* 134**,** 207-14.

Posse de Chaves, E. & S. Sipione (2010) Sphingolipids and gangliosides of the nervous system in membrane function and dysfunction. *FEBS Lett,* 584**,** 1748-59.

Rojas, R., S. Kametaka, C. R. Haft & J. S. Bonifacino (2007) Interchangeable but essential functions of SNX1 and SNX2 in the association of retromer with endosomes and the trafficking of mannose 6-phosphate receptors. *Mol Cell Biol,* 27**,** 1112-24.

Rosenthal, M. D. & R. H. Glew. 2009. *Medical Biochemistry: Human Metabolism in Health and Disease*. John Wiley & Sons, Inc.

Sadeghlar, F., K. Sandhoff & G. van Echten-Deckert (2000) Cell type specific localization of sphingomyelin biosynthesis. *FEBS Lett,* 478**,** 9-12.

Sandhoff, R. & K. Sandhoff (2018) Emerging concepts of ganglioside metabolism. *FEBS Lett*.

Sekine, Y., C. S. Siegel, T. Sekine-Konno, W. B. J. Cafferty & S. M. Strittmatter (2018) The nociceptin receptor inhibits axonal regeneration and recovery from spinal cord injury. *Sci Signal,* 11.

Siwaszek, A., M. Ukleja & A. Dziembowski (2014) Proteins involved in the degradation of cytoplasmic mRNA in the major eukaryotic model systems. *RNA Biol,* 11**,** 1122-36.

Taliaferro, J. M., M. Vidaki, R. Oliveira, S. Olson, L. Zhan, T. Saxena, E. T. Wang, B. R. Graveley, F. B. Gertler, M. S. Swanson & C. B. Burge (2016) Distal Alternative Last Exons Localize mRNAs to Neural Projections. *Mol Cell,* 61**,** 821-33.

Tang, N. & W. F. Marshall (2012) Centrosome positioning in vertebrate development. *J Cell Sci,* 125**,** 4951-61.

Tedeschi, A., S. Dupraz, C. J. Laskowski, J. Xue, T. Ulas, M. Beyer, J. L. Schultze & F. Bradke (2016) The Calcium Channel Subunit Alpha2delta2 Suppresses Axon Regeneration in the Adult CNS. *Neuron,* 92**,** 419-434.

Tracey, T. J., F. J. Steyn, E. J. Wolvetang & S. T. Ngo (2018) Neuronal Lipid Metabolism: Multiple Pathways Driving Functional Outcomes in Health and Disease. *Front Mol Neurosci,* 11**,** 10.

Tsaneva-Atanasova, K., A. Burgo, T. Galli & D. Holcman (2009) Quantifying neurite growth mediated by interactions among secretory vesicles, microtubules, and actin networks. *Biophys J,* 96**,** 840-57.

Ukleja, M., J. M. Valpuesta, A. Dziembowski & J. Cuellar (2016) Beyond the known functions of the CCR4-NOT complex in gene expression regulatory mechanisms: New structural insights to unravel CCR4-NOT mRNA processing machinery. *Bioessays,* 38**,** 1048-58.

van Echten, G., H. Iber, H. Stotz, A. Takatsuki & K. Sandhoff (1990) Uncoupling of ganglioside biosynthesis by Brefeldin A. *Eur J Cell Biol,* 51**,** 135-9.

Villanyi, Z. & M. A. Collart (2015) Ccr4-Not is at the core of the eukaryotic gene expression circuitry. *Biochem Soc Trans,* 43**,** 1253-8.

Vincenzetti, S., V. Polzonetti, D. Micozzi & S. Pucciarelli (2016) Enzymology of Pyrimidine Metabolism and Neurodegeneration. *Curr Med Chem,* 23**,** 1408-31.

Voccoli, V. & L. Colombaioni (2009) Mitochondrial remodeling in differentiating neuroblasts. *Brain Res,* 1252**,** 15-29.

Wickramasinghe, V. O., M. Gonzàlez-Porta, D. Perera, A. R. Bartolozzi, C. R. Sibley, M. Hallegger, J. Ule, J. C. Marioni & A. R. Venkitaraman (2015) Regulation of constitutive and alternative mRNA splicing

across the human transcriptome by PRPF8 is determined by 5' splice site strength. *Genome Biol,* 16**,** 201.

Yadaw, A. S., M. M. Siddiq, V. Rabinovich, R. Tolentino, R. Iyengar & J. Hansen. 2017. Lack of dynamic balance between vesicle transport and microtubule growth in neurite outgrowth enables formation of dystrophic bulbs. bioRxiv.

Yamaji, T., K. Kumagai, N. Tomishige & K. Hanada (2008) Two sphingolipid transfer proteins, CERT and FAPP2: their roles in sphingolipid metabolism. *IUBMB Life,* 60**,** 511-8.

Yu, R. K., E. Bieberich, T. Xia & G. Zeng (2004) Regulation of ganglioside biosynthesis in the nervous system. *J Lipid Res,* 45**,** 783-93.

Yu, R. K., Y. T. Tsai, T. Ariga & M. Yanagisawa (2011) Structures, biosynthesis, and functions of gangliosides--an overview. *J Oleo Sci,* 60**,** 537-44.

Zappulo, A., D. van den Bruck, C. Ciolli Mattioli, V. Franke, K. Imami, E. McShane, M. Moreno-Estelles, L. Calviello, A. Filipchyk, E. Peguero-Sanchez, T. Müller, A. Woehler, C. Birchmeier, E. Merino, N. Rajewsky, U. Ohler, E. O. Mazzoni, M. Selbach, A. Akalin & M. Chekulaeva (2017) RNA localization is a key determinant of neurite-enriched proteome. *Nat Commun,* 8**,** 583.

Zhang, H., T. Huang, Y. Hong, W. Yang, X. Zhang, H. Luo, H. Xu & X. Wang (2018) The Retromer Complex and Sorting Nexins in Neurodegenerative Diseases. *Front Aging Neurosci,* 10**,** 79.

Ziegler, W. & K. Unsicker (1981) Differential effects of cyclic AMP and cholera toxin on nerve growth factor-induced neurite outgrowth from adrenal medullary chromaffin and pheochromocytoma cells. *Brain Res,* 227**,** 622-7.

Acknowledgements: This research was supported by NIH grants R01GM54508 and Systems Biology Center grant P50GM071558.

Declaration of interests: The authors declare no competing financial interests.

Suppl. figure 1A

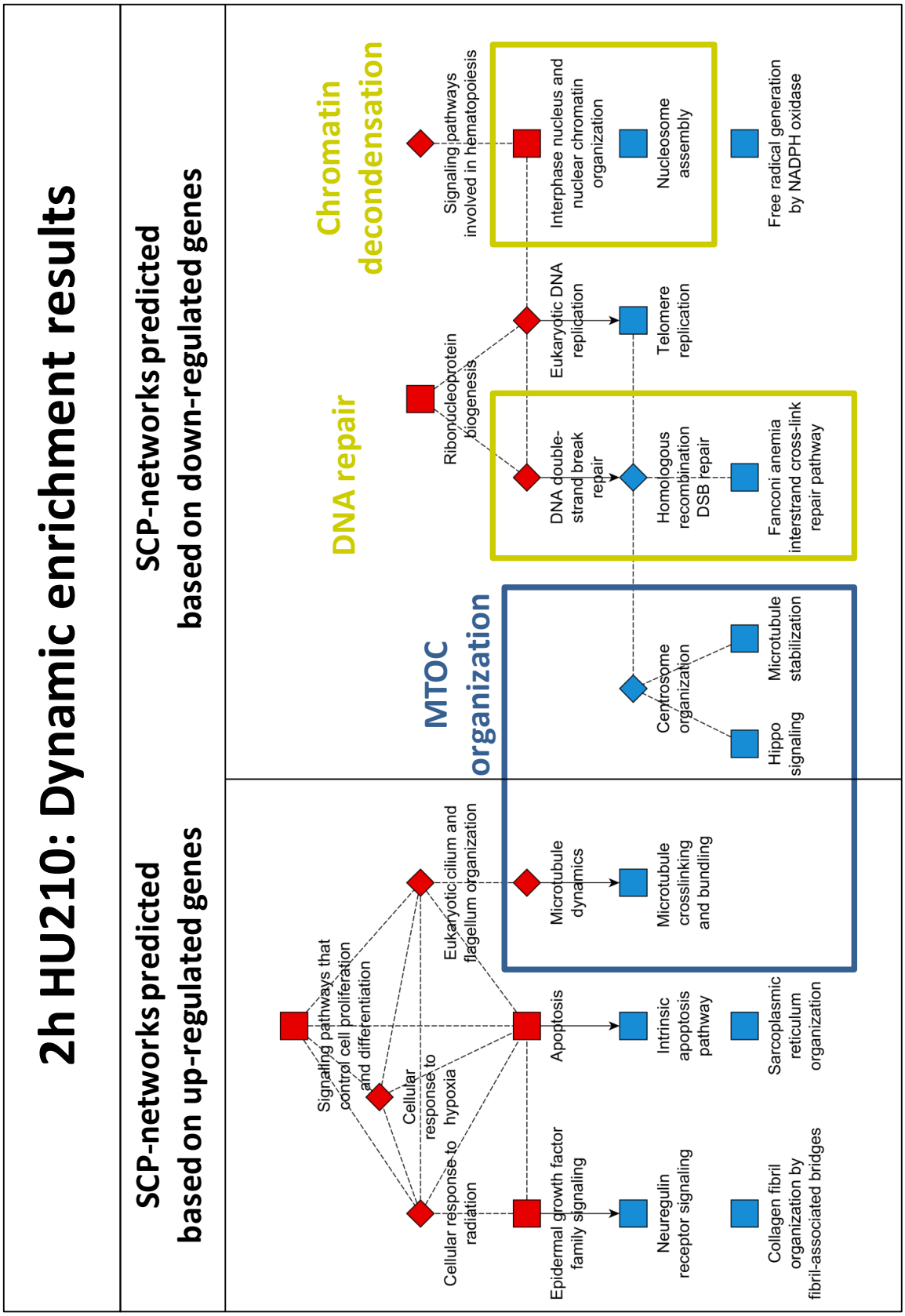

Supplementary figure 1A: Dynamic enrichment analysis of DEGS at 2h. Up- and down-regulated genes after 2h HU210 (minimum $\log_2$(fold change) of +/- $\log_2(1.5)$) were submitted to dynamic enrichment enrichment analysis using the Molecular Biology of the Cell Ontology (MBCO). Dynamic enrichment analysis considers dependencies between SCPs based on computationally predicted horizontal SCP relationships that lie within and beyond the annotated hierarchy to predict SCP-networks that describe whole cell function. Briefly, the algorithm searches for all level-2 or level-3 SCPs that contain at least one input gene and combines them to SCP-unions, if they are strongly connected. The unions are added as custom SCPs to the original set of SCPs and the new customized MBCO is used for enrichment analysis of the input genes using Fisher's Exact Test. Top three level-2 and top five level-3 predicted SCP-unions or SCPs were used to generate indicated networks. Red rectangles: level-2 SCPs, blue rectangles: level-3 SCPs. Dashed lines: horizontal SCP interactions, arrows: hierarchical annotated interactions between level-2 parent SCPs and level-3 child SCPs. MTOC: Microtubule Organization Center.

Suppl. figure 1B

2h HU210: Standard enrichment results

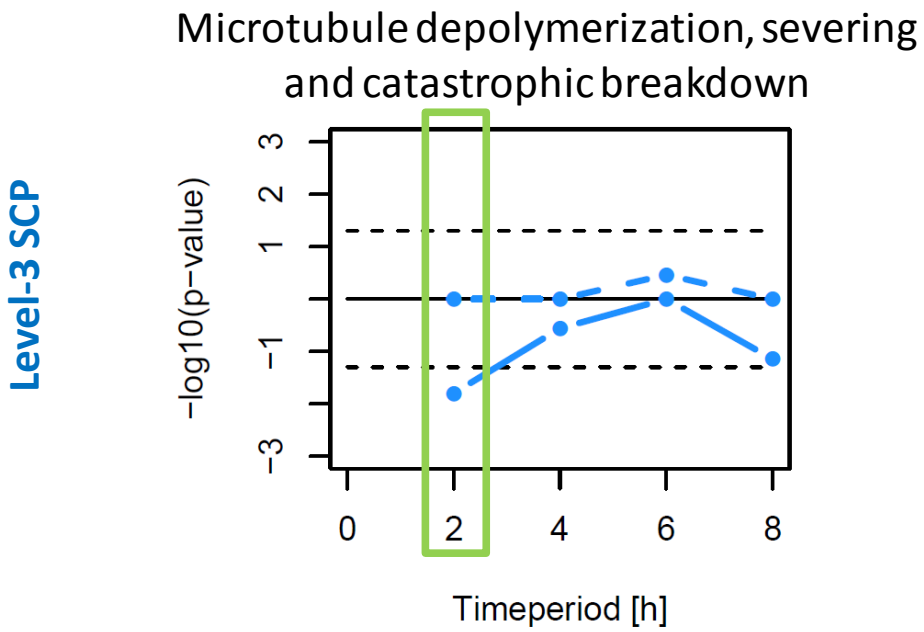

Supplementary figure 1B: Selected SCP that was predicted by standard enrichment analysis of DEGs at 2h. Up- and down-regulated genes of each timepoint (2h, 4h, 6h, 8h) with a minimum $\log_2$(fold change) of +/- $\log_2(1.3)$ were submitted to standard (regular) enrichment enrichment analysis using the Molecular Biology of the Cell Ontology (MBCO) and Fisher's Exact test. Significance was defined by a maximum nominal p-value of 5%. Minus $\log_{10}$(p-values) of the indicated SCP were plotted above 0, if they are based on enrichment results of up-regulated genes, and below 0, if they are based on enrichment results of down-regulated genes. If up- or down-regulated genes of at least one timepoint significantly enrich for that particular SCP, the minus log10(p-values) are connected by a solid line and by a dashed line otherwise. Horizontal black solid line indicates minus $\log_{10}$(p-value) of 0 (p-value=1), black dashed line indicate nominal significance threshold (minus $\log_{10}(0.05)$). Green rectangle shows the minus $\log_{10}$(p-values) of the current timepoints. See supplementary figure 2 for all predicted SCPs.

Suppl. figure 1C

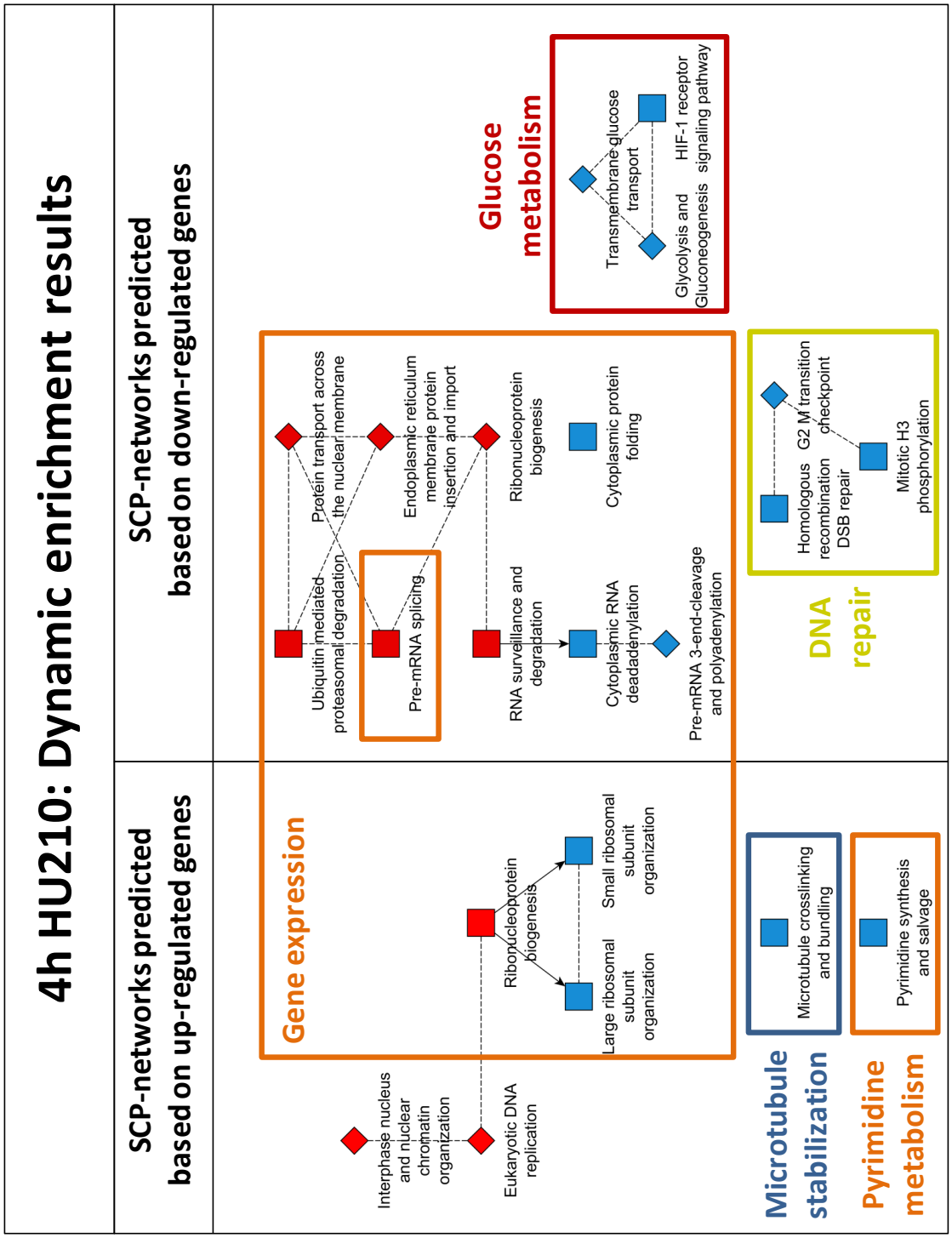

Supplementary figure 1C: Dynamic enrichment analysis of DEGs at 4h.

Suppl. figure 1D

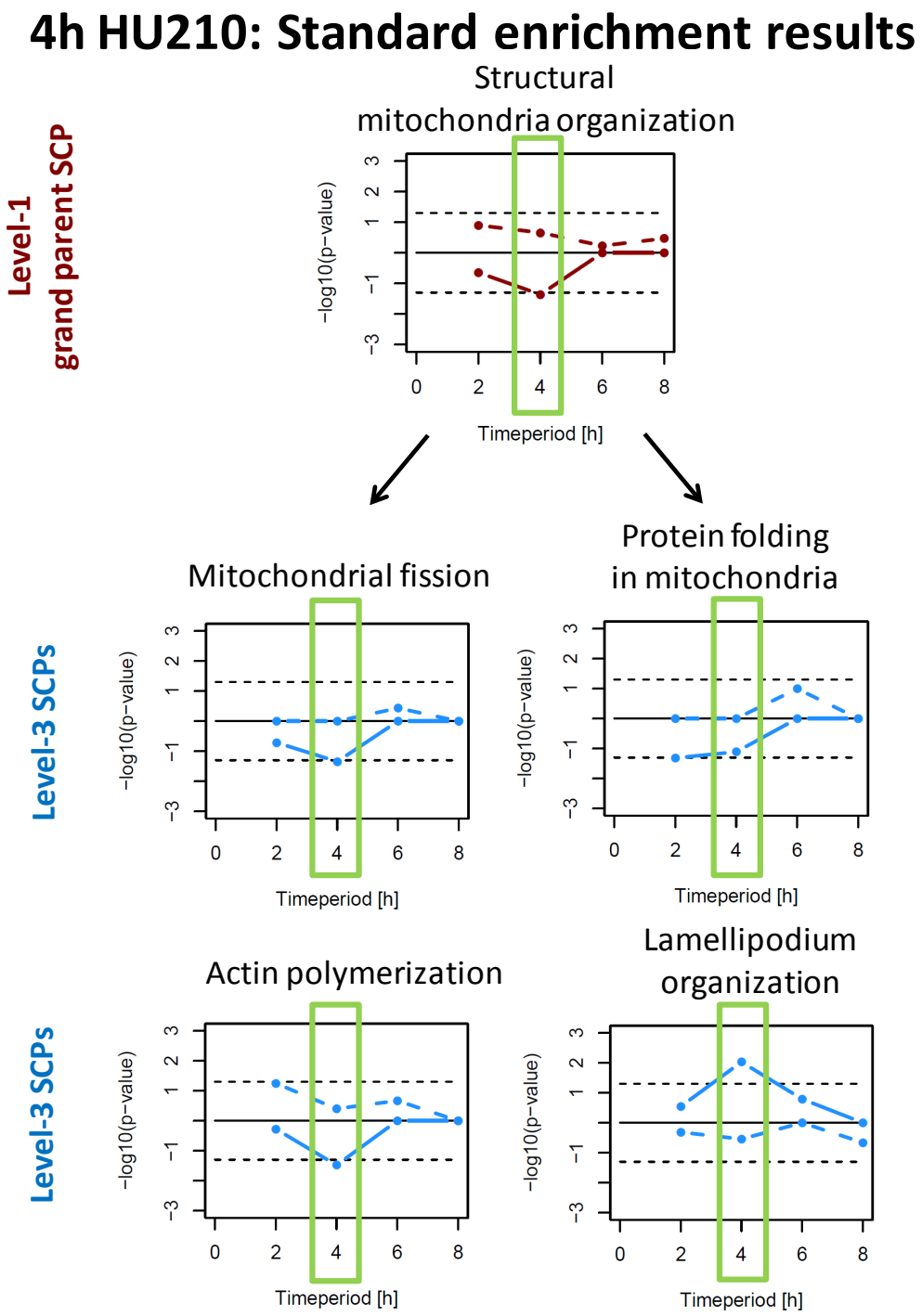

Supplementary figure 1D: Selected SCPs that were predicted by standard enrichment analysis of DEGs at 4h.

Suppl. figure 1E

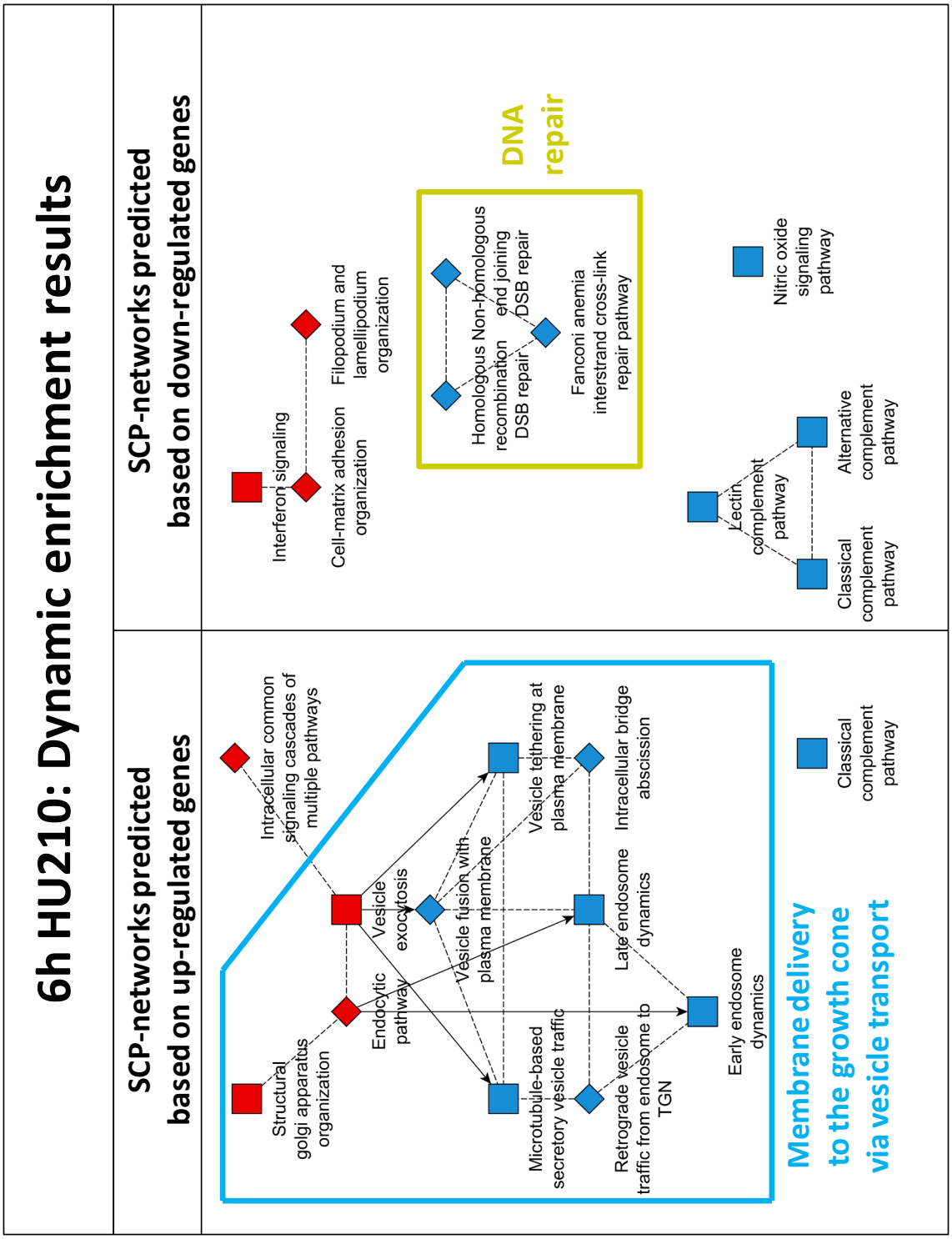

Supplementary figure 1E: Dynamic enrichment analysis of DEGs at 6h.

Suppl. figure 1F

6h HU210: Standard enrichment results

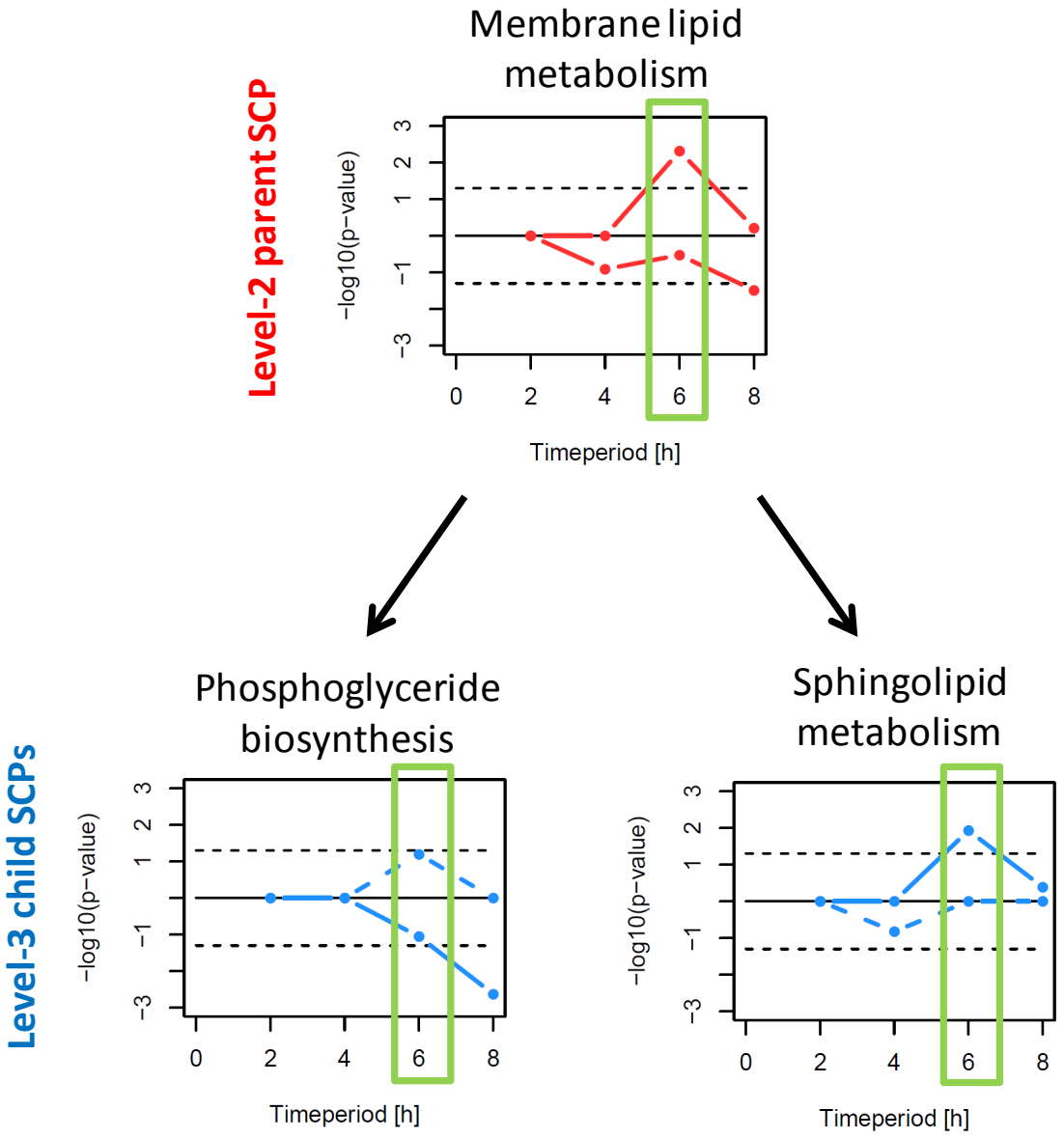

Suppl. figure 1F

6h HU210: Standard enrichment results

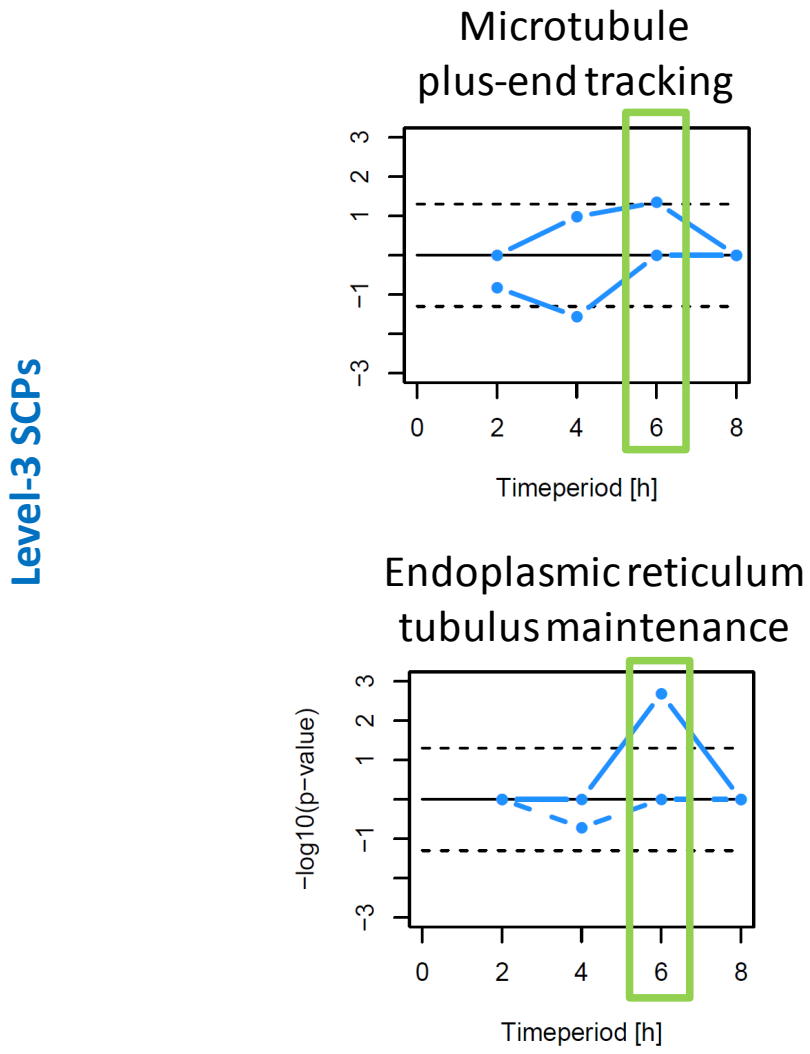

Supplementary figure 1F: Selected SCPs that were predicted by standard enrichment analysis of DEGs at 6h.

Suppl. figure 1G

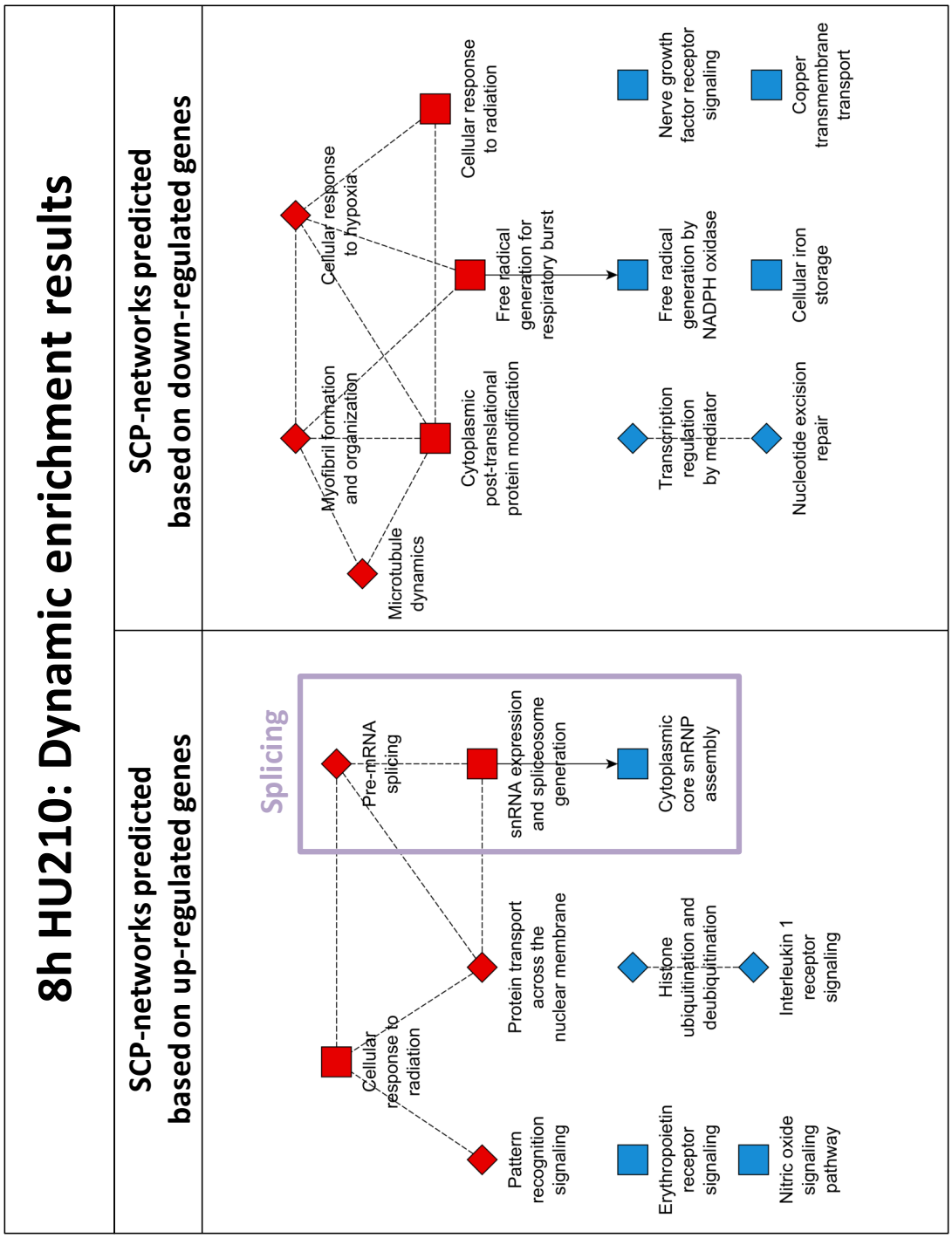

Supplementary figure 1G: Dynamic enrichment analysis of DEGs at 8h.

Suppl. figure 1H

8h HU210: Standard enrichment results

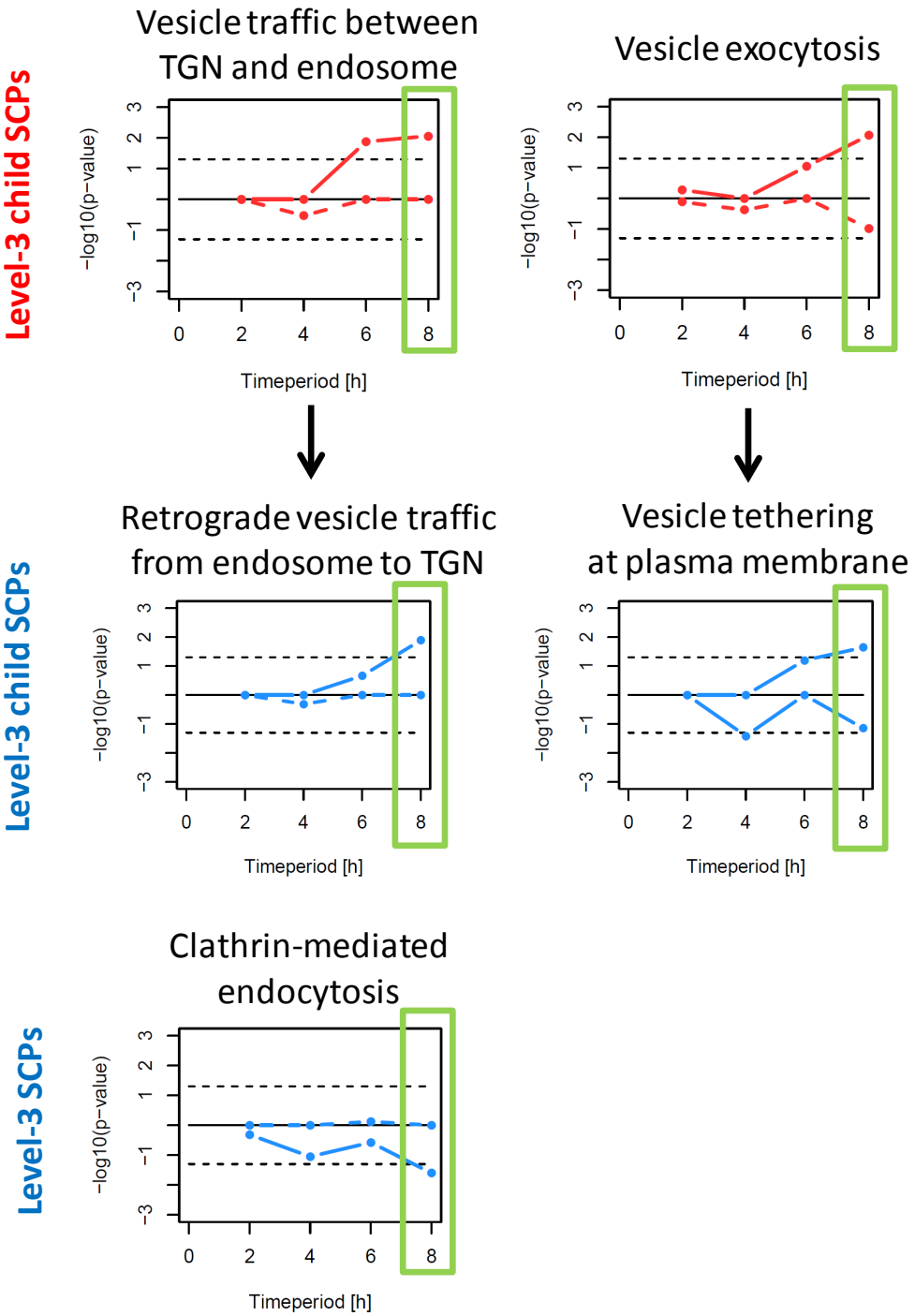

Supplementary figure 1H: Selected SCPs that were predicted by standard enrichment analysis of DEGs at 8h.

Supplementary figure 2: Timeline of all SCPs that were predicted based on standard enrichment analysis. (different PDF). First headline: Parent SCP of predicted, Second headline: predicted SCP. Dark red/light red/blue: predicted SCP is level-1/level-2/level-3 SCP. For details see supplementary figure 2B.

Supplementary table 1: Differentially expressed genes. FDR = 5%, minimum $\log_2$(fold change) = +/- $\log_2(1.3)$.

Supplementary table 2: Dynamic enrichment results of differentially expressed genes. (FDR = 5%, minimum $\log_2$(fold change) = +/- $\log_2(1.5)$). Seed supplementary figure 1A for details. The column 'Overlap symbols' lists those symbols that are part of the input gene list and the SCP. Numbers in brackets behind each symbols indicate $\log_2$(fold change) of that gene.

Supplementary table 3: Standard enrichment results of differentially expressed genes. (FDR = 5%, minimum $\log_2$(fold change) = +/- $\log_2(1.5)$). Seed supplementary figure 1B for details. The column 'Overlap symbols' lists those symbols that are part of the input gene list and the SCP. Numbers in brackets behind each symbols indicate $\log_2$(fold change) of that gene.